

RESEARCH ARTICLE

Cortical bone architecture of hominid intermediate phalanges reveals functional signals of locomotion and manipulation

Samar M. Syeda¹  | Zewdi J. Tsegai²  | Marine Cazenave^{1,3,4}  |
Matthew M. Skinner⁴  | Tracy L. Kivell⁴ 

¹Skeletal Biology Research Centre, School of Anthropology and Conservation, University of Kent, Canterbury, UK

²Department of Organismal Biology and Anatomy, University of Chicago, Chicago, Illinois, USA

³Department of Anatomy, Faculty of Health Sciences, University of Pretoria, Pretoria, South Africa

⁴Department of Human Origins, Max Planck Institute for Evolutionary Anthropology, Leipzig, Germany

Correspondence

Samar M. Syeda, Skeletal Biology Research Centre, School of Anthropology and Conservation, University of Kent, Canterbury, UK.
Email: ss2510@kent.ac.uk

Funding information

H2020 European Research Council, Grant/Award Number: 819960; HORIZON EUROPE Marie Skłodowska-Curie Actions, Grant/Award Number: 101025719

Abstract

Objectives: Reconstruction of fossil hominin manual behaviors often relies on comparative analyses of extant hominid hands to understand the relationship between hand use and skeletal morphology. In this context, the intermediate phalanges remain understudied. Thus, here we investigate cortical bone morphology of the intermediate phalanges of extant hominids and compare it to the cortical structure of the proximal phalanges, to investigate the relationship between cortical bone structure and inferred loading during manual behaviors.

Materials and Methods: Using micro-CT data, we analyze cortical bone structure of the intermediate phalangeal shaft of digits 2–5 in *Pongo pygmaeus* ($n = 6$ individuals), *Gorilla gorilla* ($n = 22$), *Pan spp.* ($n = 23$), and *Homo sapiens* ($n = 23$). The R package morphomap is used to study cortical bone distribution, cortical thickness and cross-sectional properties within and across taxa.

Results: Non-human great apes generally have thick cortical bone on the palmar shaft, with *Pongo* only having thick cortex on the peaks of the flexor sheath ridges, while African apes have thick cortex along the entire flexor sheath ridge and proximal to the trochlea. Humans are distinct in having thicker dorsal shaft cortex as well as thick cortex at the disto-palmar region of the shaft.

Discussion: Variation in cortical bone distribution and properties of the intermediate phalanges is consistent with differences in locomotor and manipulative behaviors in extant great apes. Comparisons between the intermediate and proximal phalanges reveals similar patterns of cortical bone distribution within each taxon but with potentially greater load experienced by the proximal phalanges, even in knuckle-walking African apes. This study provides a comparative context for the reconstruction of habitual hand use in fossil hominins and hominids.

KEYWORDS

cortical bone, functional morphology, hominin manual behaviors, internal bone structure, phalangeal morphology

This is an open access article under the terms of the [Creative Commons Attribution](https://creativecommons.org/licenses/by/4.0/) License, which permits use, distribution and reproduction in any medium, provided the original work is properly cited.

© 2024 The Authors. *American Journal of Biological Anthropology* published by Wiley Periodicals LLC.

1 | INTRODUCTION

Extant great apes and modern humans use a range of hand postures during positional (locomotor and postural) and manipulative behaviors (e.g., Kivell et al., 2020; Schmitt et al., 2016), which have been successfully linked to the morphological variation within great ape hands (Bird et al., 2021, 2022; Dunmore et al., 2019; Dunmore, Bardo, et al., 2020; Dunmore, Skinner, et al., 2020; Marchi, 2005; Matarazzo, 2008, 2015; Tsegai et al., 2013). This form-function link among extant taxa has been used to infer habitual manual activities of fossil taxa, ranging from Miocene apes (Almecija et al., 2009; Almécija et al., 2012; Susman, 2004) to fossil *Homo sapiens* (Bardo et al., 2020; Kivell et al., 2022; Stephens et al., 2018). Recent discoveries of hominin hand fossils have revealed mosaic morphologies suggesting hand use during both arboreal locomotion and dextrous manipulation (Dunmore, Skinner, et al., 2020; Kivell et al., 2015, 2018). Notably, the manual intermediate phalanges within the hominin fossil record show a mix of primitive and derived morphologies that suggest a diverse range of manual behaviors during the evolution of the hominin hand (Alba et al., 2003; Haile-Selassie & WoldeGabriel, 2009; Kivell et al., 2015, 2018, 2020; Larson et al., 2009; Napier, 1962; Susman & Creel, 1979). Functional inferences regarding manual behaviors of these fossil specimens have been made using elements of the carpus (Kivell et al., 2013; Marzke et al., 2010; Tocheri et al., 2007), the metacarpus (Dunmore, Skinner, et al., 2020; Galletta et al., 2019; Skinner et al., 2015) and the phalanges (Almecija et al., 2010; Kivell et al., 2015, 2018, 2022; Syeda et al., 2022), but the intermediate phalanges are relatively understudied. Here we build on our previous work (Syeda et al., 2023) and investigate variation in cortical bone structure of the intermediate phalanges of digits 2–5 (IP2–IP5) within the context of inferred hand use in humans and other extant hominids (*Pongo*, *Gorilla*, and *Pan*). We also conduct intra-digit comparisons of both the proximal and intermediate phalanges and discuss how the combined cortical structure of these two elements may reflect function of the fingers during manual behaviors.

Phalangeal external morphology, as well as the internal bone structure, have been shown to be functionally informative (Jungers et al., 1997; Karakostis et al., 2018; Matarazzo, 2008; Patel & Maiolino, 2016; Susman, 1979; Syeda et al., 2023). The structure of both cortical and trabecular bone can adapt in response to mechanical loading by removing bone in skeletal areas where stress is low and adding bone where stress is high (Barak et al., 2011; Currey, 2013; Pearson & Lieberman, 2004; Ruff et al., 2006) as well as by changing the orientation and alignment of the trabecular struts (Barak et al., 2011; Pontzer et al., 2006). Preserved cortical and trabecular architecture of fossil specimens of different limb elements has been used to infer locomotor behavior and manipulative activities (e.g., Cazenave et al., 2019; Chirchir, 2019; Dunmore, Skinner, et al., 2020; Georgiou et al., 2020; Ruff et al., 2016; Skinner et al., 2015; Su & Carlson, 2017; Zeininger et al., 2016; see also the review in Cazenave & Kivell, 2023). These behavioral reconstructions rely on understanding the relationship between bone structure and known behaviors of extant taxa.

1.1 | External morphology of the intermediate phalanges

Among great apes, external morphology of the intermediate phalanges is variable in the degree of longitudinal curvature, shape of the base, shaft, and trochlea, as well as a suite of morphological features on the palmar surface (Marzke et al., 2007; Patel & Maiolino, 2016; Susman, 1979; Syeda et al., 2021). These palmar morphological features include a median bar, lateral fossae, and the flexor sheath ridges (FSRs) (Figure 1). The median bar typically runs along the length of the palmar shaft with lateral fossae on either side and that are bounded by the FSRs (Marzke et al., 2007; Susman, 2004). The lateral fossae of the intermediate phalanges are traditionally thought to be attachment sites for the flexor digitorum superficialis (FDS) muscle (Marzke et al., 2007) and the size, depth and shape of these are quite variable across great apes (Susman, 1979) and throughout the fossil hominin record (Alba et al., 2003; Bush et al., 1982; Haile-Selassie & WoldeGabriel, 2009; Kivell et al., 2015, 2018, 2020; Larson et al., 2009; Napier, 1962; Pickering et al., 2018; Susman & Creel, 1979; Ward et al., 2012). The relative size and overall morphology of these fossae have been used to make functional inferences regarding the locomotion of fossil hominins (Bush et al., 1982; Day, 1978; Ricklan, 1987; Stern & Susman, 1983; Susman, 1979; Susman & Creel, 1979; Susman & Stern, 1979; Tuttle, 1981). The deep lateral fossae of *Australopithecus afarensis* and *Australopithecus africanus* intermediate phalanges have been interpreted as evidence of efficient power grasping, which would have allowed them to engage in climbing and suspensory locomotion despite having short fingers, with *A. africanus* also potentially participating in tool using activities (Ricklan, 1987; Stern & Susman, 1983; Susman et al., 1984). Similar inferences have been made for the intermediate phalanges of the OH 7 *Homo habilis* hand (Susman & Creel, 1979). While these previous studies have linked FSR morphology to the size and use of the FDS muscles, there is a lack of evidence linking the morphology of muscle attachment sites and the size of the muscle (Shrewsbury et al., 2003; Williams-Hatala et al., 2016; but see Karakostis et al., 2017). Furthermore, as the morphology of the intermediate phalanges is understudied, the functional implications of the variation observed in FSR morphology and the palmar median bar have remained relatively unexplored.

1.2 | Functional morphology of the intermediate phalanges

To date, only two studies, of which we are aware, have directly investigated the biomechanical and behavioral implications of palmar phalangeal morphology (Marzke et al., 2007; Nguyen et al., 2014). In a comparative anatomical study of primate intermediate phalanges, Marzke et al. (2007) showed that the FDS tendon does not exclusively insert onto the lateral fossae and, when it does, it does not occupy the whole fossa. Instead, the FDS tendon mainly inserted onto the FSRs at varying distances from the base, with the fibers running

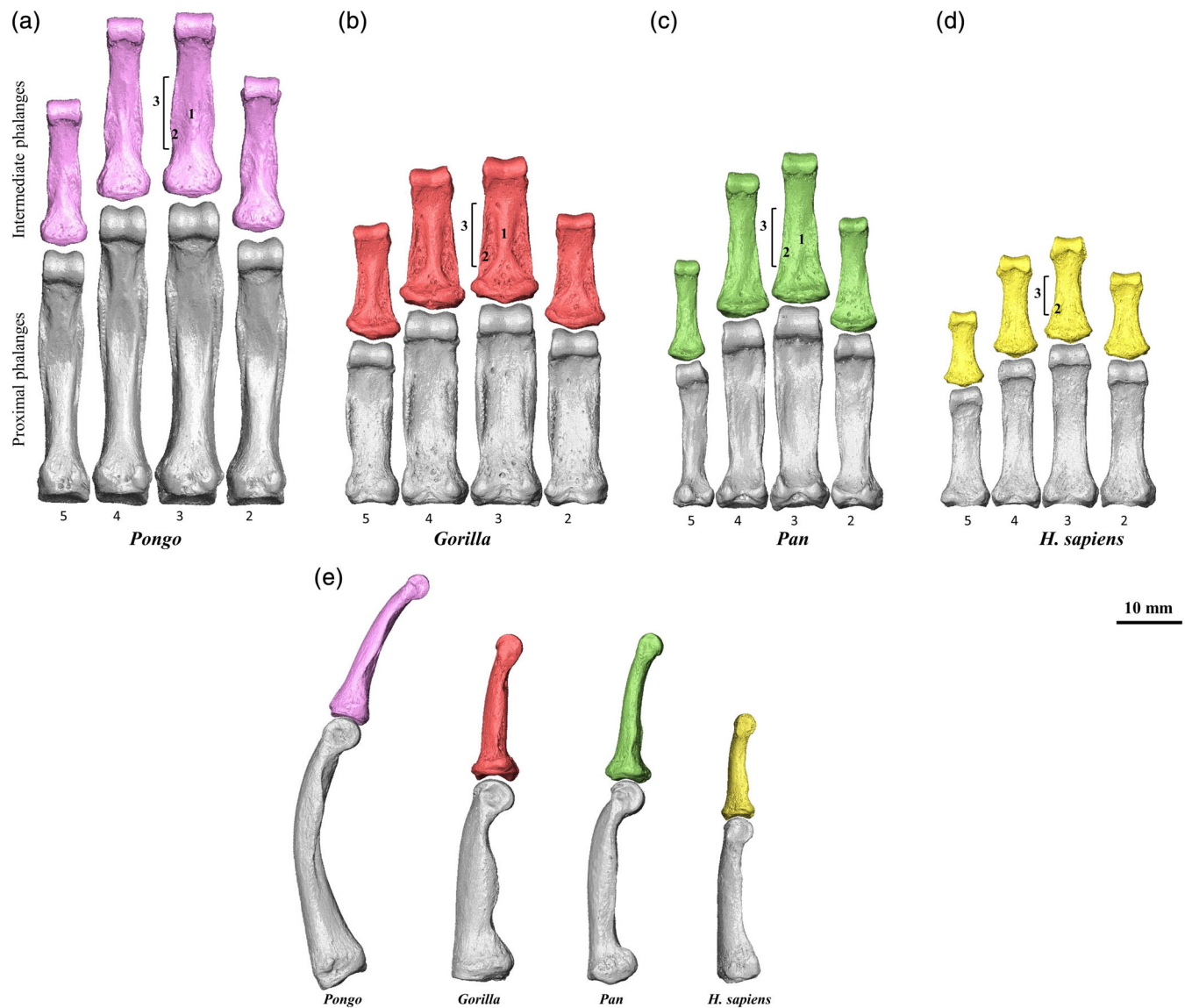


FIGURE 1 Surface models derived from micro-CT scans of proximal and intermediate phalanges of digits 2–5 from (a) *Pongo pygmaeus*, (b) *Gorilla gorilla*, (c) *Pan troglodytes*, and (d) *Homo sapiens* showing variation in external morphology. External morphological features are labeled: 1: Palmar median bar, 2: Lateral fossae, and 3: flexor sheath ridge. (e) Proximal and intermediate phalanges of the third digit in the ulnar view to demonstrate variation in longitudinal curvature across the sample.

towards different aspects of the palmar shaft (Marzke et al., 2007). The length of the lateral fossae also did not predict the cross-sectional area or length of the FDS tendon, concluding that the development of this external morphology cannot be explained by the FDS tendon attachments or the stresses associated with FDS muscle activity (Marzke et al., 2007). An alternative explanation of lateral fossae development proposed by Marzke et al. (2007) is that the lateral fossae could be a by-product of the median bar thickening and developing anteriorly in response to loading. This hypothesis is consistent with Begun et al. (1994) study of the pedal intermediate phalanges of *Proconsul* in which they posited that the palmar median bar reflects dorsopalmarly directed bending stresses that accompany the contraction of the power digital flexor muscles and substrate reaction forces. In contrast, Walker et al. (1993) suggested that the

palmar median bar could form as a result of the lateral fossae excavations, however, this hypothesis requires a functional explanation for the hollowing out of the palmar phalangeal shaft. While Marzke et al. (2007) focused on the shape and size of the lateral fossae, they did not explicitly explain or address the functional role and morphology of the FSRs. The work of Nguyen et al. (2014) sheds light on the biomechanical importance of the FSRs in the proximal phalanx of hylobatids. Using 3D microfinite element modeling, they showed that the larger FSRs experienced higher peak strains and were associated with lower peak strains on the palmar shaft, suggesting that taller FSRs helped to reduce the strain experienced by the palmar shaft (Nguyen et al., 2014). If the same is true for intermediate phalanges, this may help to explain variation in FSR development across hominoid taxa.

Variation in hominoid external intermediate phalangeal shape, especially regarding phalangeal curvature, FSR morphology and soft tissue anatomy, make functional interpretations in extant and fossil phalangeal form challenging. However, exploration of internal bone structure may provide more direct information about finger use. To date, only three studies have investigated the functional relationship between the internal bone morphology of intermediate phalanges and hand use behaviors (Doden, 1993; Matarazzo, 2015; Stephens et al., 2018). Doden (1993) showed that the intermediate phalanges of modern humans have thinner cortical bone towards the distal end, with overall thicker cortical bone on the dorsal surface of the phalanx and the midshaft having the highest density of bone. Matarazzo (2015) and Stephens et al. (2018) studied the trabecular structure of catarrhine and modern human phalanges, respectively, and noted a functional link between manual behaviors and the orientation and volume of trabecular bone.

We previously explored cortical bone distribution patterns and properties in the proximal phalanges of digits 2–5 (PP2–PP5) in extant great apes and showed that the pattern of cortical bone within the non-pollical proximal phalanges is capable of distinguishing varied hand postures employed by each taxon and corresponds with predicted loading during these hand postures (Syeda et al., 2023). Results also indicated that cortical bone patterns and properties reflect the variable digital loading within the hand of each taxon (Syeda et al., 2023). Here, we build upon this research and provide the first detailed, comparative study of the cortical morphology of extant hominid intermediate phalanges in digits 2–5. We examine cortical bone distribution patterns and cortical robusticity via cross-sectional geometry (CSG) in the phalangeal shaft to test whether these cortical properties reflect predicted loading differences during manual behaviors. We then discuss the cortical bone morphology of the intermediate phalanges alongside the proximal phalanges to provide a more holistic insight into the relationship between phalangeal morphology and hominid hand use.

1.3 | Predictions

1.3.1 | Inter-specific comparisons of cortical bone structure

We predict cortical bone distribution patterns will differ among the extant great apes, reflecting the presumed loading associated with the typical hand postures employed by each taxon. *Pongo* locomotor repertoire is dominated by suspensory, arboreal behaviors (Hunt, 1991; Thorpe & Crompton, 2006; but see Sarmiento, 1988; Susman, 1974; Tuttle, 1967) in which the hand wraps around the substrate using flexed-finger postures. We predict that the intermediate phalanges of *Pongo* will display a pattern of thick cortical bone on the midshaft-to-distal palmar surface, as the flexed finger posture of the phalanges will result in joint and substrate reaction forces that will load the phalanx in compression dorsally and tension palmarly, with the FSRs and longitudinal curvature of the phalanx helping reduce

overall strain experienced by the shaft (Nguyen et al., 2014; Preuschoft, 1973; Richmond, 2007).

The African apes (*Gorilla* and *Pan*) most often engage in knuckle-walking (on average ~90% of time spent locomoting, but this can vary substantially across groups and individuals; Hunt, 2020) and, less often, in arboreal behaviors (Doran, 1996, 1997; Hunt, 2020; Remis, 1998; Schaller, 1963; Tuttle & Watts, 1985). During knuckle-walking, the intermediate phalanges contact the substrate with the dorsal surface, the metacarpophalangeal (McP) joint is hyperextended, the PIP joint is hyperflexed, and the DIP joint is flexed (Inouye, 1994; Matarazzo, 2013; Thompson, 2020; Thompson et al., 2018; Tuttle, 1967). We predict *Gorilla* and *Pan* will share a similar pattern of cortical bone distribution, with an overall thick phalangeal shaft due to ground reaction forces being dissipated on the dorsal surface and large compressive forces from supporting body mass during knuckle-walking (Matarazzo, 2015; Wunderlich & Jungers, 2009).

Modern humans primarily use their hands for manipulation, employing power grips frequently, as well as power squeeze grips and precision grips between the finger pads and thumb (Dollar, 2014; Feix et al., 2015; Zheng et al., 2011). These grips most often result in flexion at the fingers, which will result in compressive and bending stresses on the dorsal surface of the relatively straight phalanges (Doden, 1993; Marzke, 1997; Preuschoft, 1973; Zheng et al., 2011). As such, we expect humans to have the thickest cortex on the dorsal surface of the phalanx.

Along with differences in cortical distribution patterns, we predict there will be differences in cortical thickness values across the phalanx and cross-sectional geometric (CSG) properties across the taxa. It is predicted the African apes will have relatively thicker mean cortical thickness and higher cross-sectional properties compared to *Pongo* and *H. sapiens*. *Pongo* will display cortical bone thickness and properties that are intermediate between the African apes and modern humans, as the gravitational forces associated with below-branch manual postures will be distributed across all three phalanges in each digit and thus loads experienced directly by the intermediate phalanx will be lower than those incurred during knuckle-walking. Human intermediate phalanges are predicted to have the thinnest cortices and weakest CSG properties compared to the other taxa, as the lower loads experienced during manipulation are predominant in humans and loading during locomotion is likely to be negligible in the human sample used in this study.

1.3.2 | Intra-specific comparisons of cortical bone structure

Given differences in loading among the digits during habitual hand postures, we also predict that cortical bone distribution, mean thickness and CSG properties will differ across the digits within each taxon. Within the African apes, captive *Gorilla* has been observed to load its digits 2–5 more evenly (but see Thompson et al., 2018) compared to captive *Pan*, which is more variable in its positional behavior (Doran, 1996; Doran & Hunt, 1996; Hunt, 1992; Inouye, 1994;

Matarazzo, 2013; Sarringhaus et al., 2014; Tuttle, 1969). Generally, in *Pan* digits 3 and 4 experience the greatest loads and digit 5 sometimes does not even touch down while knuckle-walking (Matarazzo, 2013; Samuel et al., 2018; Wunderlich & Jungers, 2009). Thus, *Gorilla* is predicted to have similar cortical bone distribution and properties across digits 2–5 while *Pan* is predicted to be more variable with greater cortical bone thickness and properties in the third digit (Samuel et al., 2018; Wunderlich & Jungers, 2009). In *Pongo*, cortical distribution, mean thickness and CSG properties are expected to be similar across the digits since *Pongo* is thought to typically use all four fingers in a similar manner during arboreal grasping (Rose, 1988; but see McClure et al., 2012). Within modern humans, we expect digit 2 and 3 to have thicker cortices and stronger CSG properties than digits 4 and 5 as experimental studies have shown greatest loads are experienced by the radial digits during modern human grasping (Cepriá-Bernal et al., 2017; De Monsabert et al., 2012; Sancho-Bru et al., 2014).

1.3.3 | Comparison of proximal and intermediate phalanges

We expect to observe similar relative patterns and interspecific differences in cortical morphology of the intermediate phalanges that we did in the proximal phalanges (PPs) (Syeda et al., 2023). Specifically, we expect *Pongo* and *H. sapiens* to show similar patterns between their respective IPs and PPs, while African apes will show greater differences between their phalangeal elements due to direct loading of the IPs during knuckle-walking.

2 | METHODS

2.1 | Sample

This study included high resolution micro-CT scans of intermediate phalanges of modern *H. sapiens* ($n = 23$ individuals, including recent and early modern specimens), *Pan* spp. ($n = 23$ individuals), *Gorilla gorilla* ($n = 22$ individuals), and *Pongo pygmaeus* ($n = 6$ individuals) for manual digit 2 ($n = 56$ elements), digit 3 ($n = 62$ elements), digit 4 ($n = 64$ elements), and digit 5 ($n = 53$ elements) (Table 1). Non-human specimens were adult wild-shot individuals with no indication of pathologies and included associated intermediate phalanges (IP) of digits 2–5 from a single hand. The human sample consists of adults

TABLE 1 Summary of the sample included in the study.

Taxon	N	IP2	IP3	IP4	IP5
<i>Homo sapiens</i>	23	15	19	18	1
<i>Pan paniscus</i>	6	6	5	6	5
<i>Pan troglodytes</i>	17	11	13	15	14
<i>Gorilla gorilla</i>	22	18	19	19	16
<i>Pongo pygmaeus</i>	6	6	6	6	5

from pre-industrial ($n = 6$) and post-industrial ($n = 7$) modern human populations, as well as nine fossil *H. sapiens* specimens (further detail on populations and fossil specimens are provided in Table S1). The majority (74%) of our human sample did not have all four associated digits and therefore we assigned phalanges to a digit using morphological characteristics described in Susman (1979) and Case and Heilman (2006). For individuals in our sample that had associated PPs (see Syeda et al., 2023), we compared cortical distribution and properties with the IPs.

2.2 | MicroCT data collection

Specimens were scanned using a BIR ACTIS 225/300, Diondo D3 or Skyscan 1172 scanner housed at the Department of Human Evolution, Max Planck Institute for Evolutionary Anthropology (Leipzig, Germany), a Nikon 225/XTH scanner at the Cambridge Biotomography Centre, University of Cambridge (Cambridge, UK), or with the Diondo D1 scanner at the Imaging Centre for Life Sciences University of Kent (Canterbury, UK). The scan parameters included acceleration voltages of 100–160 kV and 100–140 μ A using a 0.2–0.5 mm copper or brass filter. Scan resolution ranged between 0.018 and 0.044 mm depending on the size of the bone. Images were reconstructed as 16-bit TIFF stacks. All scans were cleaned (i.e., the removal of soft tissue or other non-bone material) and reoriented into a standard anatomical position using Avizo Lite 9.0.0 (Visualization Sciences Group, SAS). These scans were then segmented using medical image analysis (MIA), a clustering algorithm method (Dunmore et al., 2018).

2.3 | Analysis of cortical bone structure

The R package morphomap (Profico et al., 2021) was used to quantify cortical bone structure distribution and CSG properties. To prepare the data for analysis, we used Medtool v 4.5 (www.dr-pahr.at/medtool; Gross et al., 2014; Tsegai et al., 2013) on the original and MIA segmented scans, to define the inner and outer layer of cortical bone in the segmented scans. The protocol identified the external and internal border by casting rays in 3D and used morphological filters to fill the bone, which resulted in masks of the outer and inner region of cortical bone. These masks were converted into smooth external and internal surfaces for processing in morphomap using an in-house script for Paraview v 4.4 and Meshlab v 2020.03.

Prior to analysis, we extracted a region of interest (ROI) from the inner and outer surfaces that defined the phalangeal shaft in all taxa. This ensured that the cortical region analyzed was homologous across the morphologically variable phalangeal shafts of the hominid sample. The ROI was defined distally by the proximal end of the trochlea and proximally by the distal end of the base. Cortical morphology was quantified using the R package morphomap (Profico et al., 2021) and the methodological steps and parameters applied were following Syeda et al. (2023). Briefly, 97 cross sections were extracted between 2% and 98% of the length of the ROI at 1% increments and 50 equian-gular semi-landmarks were placed on each cross-section to capture

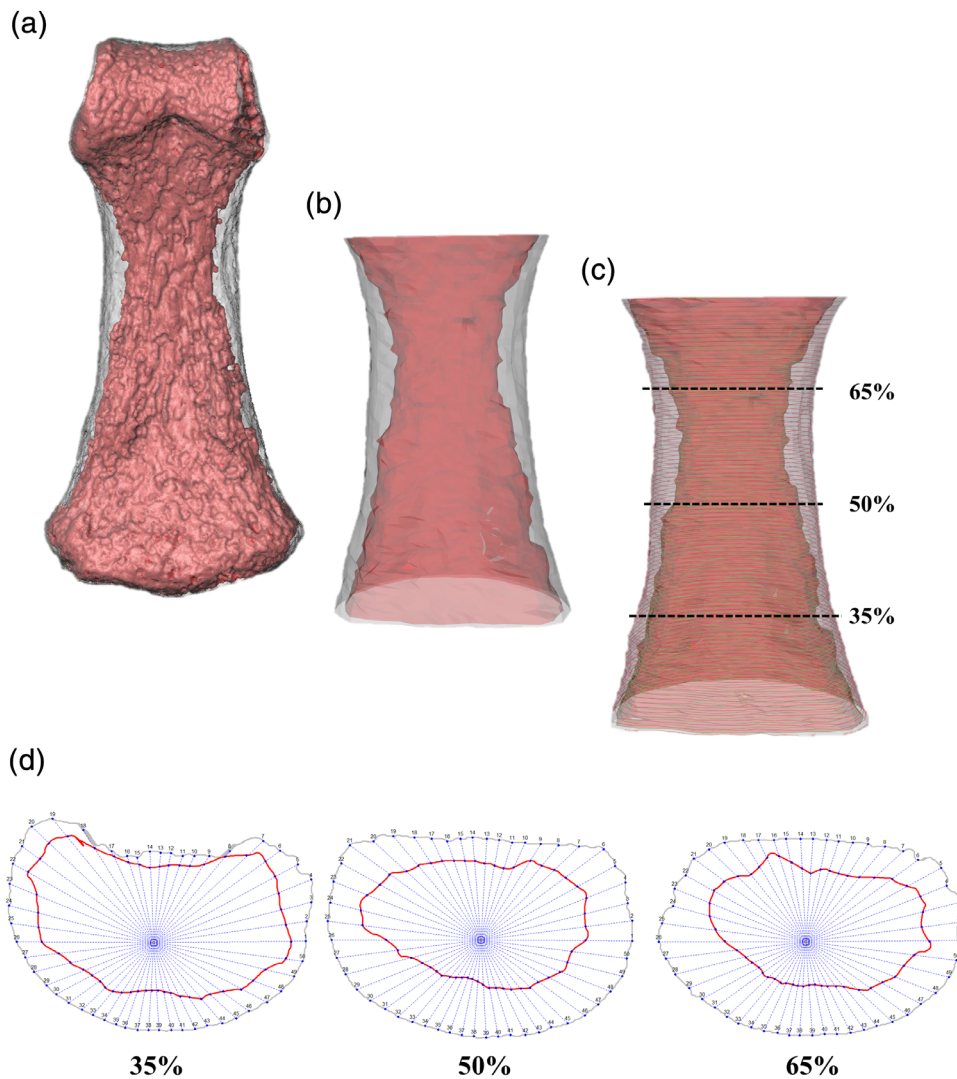


FIGURE 2 Images showing the steps taken in morphomap for cortical bone analysis in a human third intermediate phalanx. (a) External (gray) and internal (red) 3D surface model of the phalanx, (b) cut external and internal surfaces defining the ROI for input into morphomap, (c) cross-sections placed in 1% increments along the shaft to calculate cortical thickness with the dotted black lines indicating the cross-sectional levels at which cross-sectional properties were assessed, and (d) cross-sections at 35%, 50%, and 65% of the phalanx, depicting the landmarks placed on the external and internal outline.

the morphologically complex shape of the phalangeal shaft (Figure 2). To define these landmarks, rays were sent from the centroid of each cross-section outward, with cortical thickness calculated as the length of the segment between the landmarks placed on the internal and external outline. Morphometric maps of cortical bone distribution were used to visualize cortical bone distribution patterns for each individual. Mean morphometric maps were also created to visualize the overall pattern of cortical bone distribution of each digit within each taxon. To compare cortical thickness between the dorsal and palmar shaft, equiangular semi-landmarks were defined that excluded those placed on the flexor sheath ridges, that would bias measurements, and a ratio of dorsal to palmar mean cortical thickness was calculated.

2.4 | External morphological features

External morphological features (i.e., FSRs, median bar and phalangeal curvature depicted in Figure 1) of the intermediate phalanx were quantified to explore the potential relationship between external form and internal cortical architecture. We quantified phalangeal curvature

using the included angle method (Stern et al., 1995). The size of the median bar and FSRs was quantified using 3D metric measurements (Avizo Lite 9.0.0, Visualization Sciences Group, SAS). The size of the median bar was quantified from the palmar most protruding part of the bar to the palmar shaft (Figure S6). The size of the FSRs was quantified by measuring its depth (tallest point of the ridge to the palmar shaft) and its proximodistal length. The relationship between FSR and median bar morphology was only quantified in the IP3s of our sample.

2.5 | Cross-sectional geometry

Cross-sectional geometric properties quantifying the strength and rigidity of the phalangeal shaft of great apes were calculated across the shaft using morphomap (Profico et al., 2021). We analyzed cortical area (CA; measure of compressive and tensile strength), polar section modulus (Z_{pol} ; measure of maximum bending strength), and polar moment of area (J ; a measure of bending and torsional rigidity) at 35%, 50%, and 65% of the phalangeal length (Figure 3) to quantify variation in cortical bone strength properties across the phalangeal shaft.

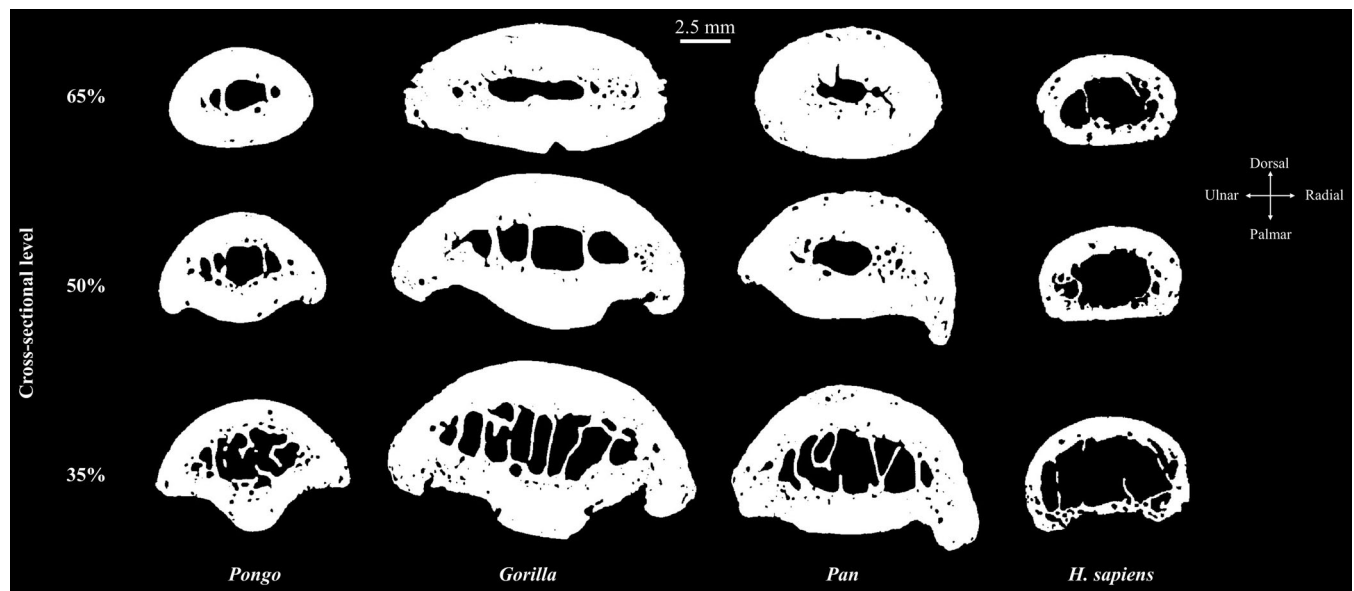


FIGURE 3 Cross-sections at 35%, 50%, and 65% of a third intermediate phalanx for each taxon. Cross-sections are scaled to relative size.

2.6 | Statistical analysis

Cortical bone thickness values, CSG properties, and metric measurements of the palmar shaft morphology were scaled by the inter-articular length of the phalanx. We also scaled our data by a geometric mean of several measurements of phalanx size, which yielded the same overall results. Thus, we chose to use phalangeal length alone to scale our data due to its direct relationship with bending stresses. First, to investigate cortical bone distribution patterns across the taxa, a principal component analysis (PCA) was conducted on the cortical thickness values of the entire shaft using R function *prcomp*. The PCA extremes were calculated from the results of the PCA, with the loadings at ± 2 standard deviations for each PC axis added to the mean morphometric map at each cell. Following the PCA, an omnibus permutational multivariate analysis of variance was conducted on the first three PC scores to test if these cortical bone distribution patterns were significantly different across the taxa. If results were statistically significant ($p < 0.05$), a pairwise one-way permutational multivariate analysis of variance with a Bonferroni correction was used to determine significant differences between the groups.

Second, to test for differences in cortical bone thickness of the shaft, mean differences were compared inter- and intra-generically using Kruskal–Wallis and post hoc Dunn tests. Wilcoxon signed-rank tests were conducted on the mean palmar and dorsal cortical thickness values to test whether they statistically differed. Regression analyses were used to assess whether a statistically significant relationship exists between cortical thickness of the shaft and degree of phalangeal curvature, as well as between cortical thickness and median bar height.

Additionally, each cross-sectional property (CA, Z_{pol} , and J) was analyzed at each cross-section (35%, 50%, and 65%) to test for inter- and intra-generically mean differences using Kruskal–Wallis and post hoc

Dunn tests. Further intra-generically testing evaluated mean differences in cross-sectional properties (CA, Z_{pol} , and J) within a phalanx at the different cross-sectional levels (35%, 50%, and 65%) using a Kruskal–Wallis test, followed by a post hoc Dunn test.

Finally, we compared cortical morphology of the intermediate phalanges with associated proximal phalanges, analyses of which were reported in our previous study (Syeda et al., 2023). The same data collection protocol was used to quantify cortical thickness in both the intermediate and proximal phalanges to ensure comparable results. We used Wilcoxon signed-rank tests to evaluate intra-generically mean differences in cortical thickness and cross-sectional properties between proximal and intermediate phalanges. We tested whether the mean cortical thickness of proximal and intermediate phalanges was significantly different across digits 2–5 of each taxon. The same tests were conducted for each cross-sectional property at each cross-section as well.

All statistical analysis was performed in R (v 4.1.3) and packages RVAideMemoire (v 0.9-79 Hervé, 2022), Stats (R Core Team, 2021), Vegan (v 2.5-7 Oksanen et al., 2020), and FSA (v 0.9.3 Ogle et al., 2022) were used.

3 | RESULTS

3.1 | Cortical bone distribution pattern and thickness

Mean morphometric maps of cortical bone distribution patterns in IP2–5 for each taxon are shown in Figure 4 and mean thickness data are presented in Table 2. Below we describe in detail the cortical bone distribution patterns and variation in scaled mean cortical thickness values for each taxon.

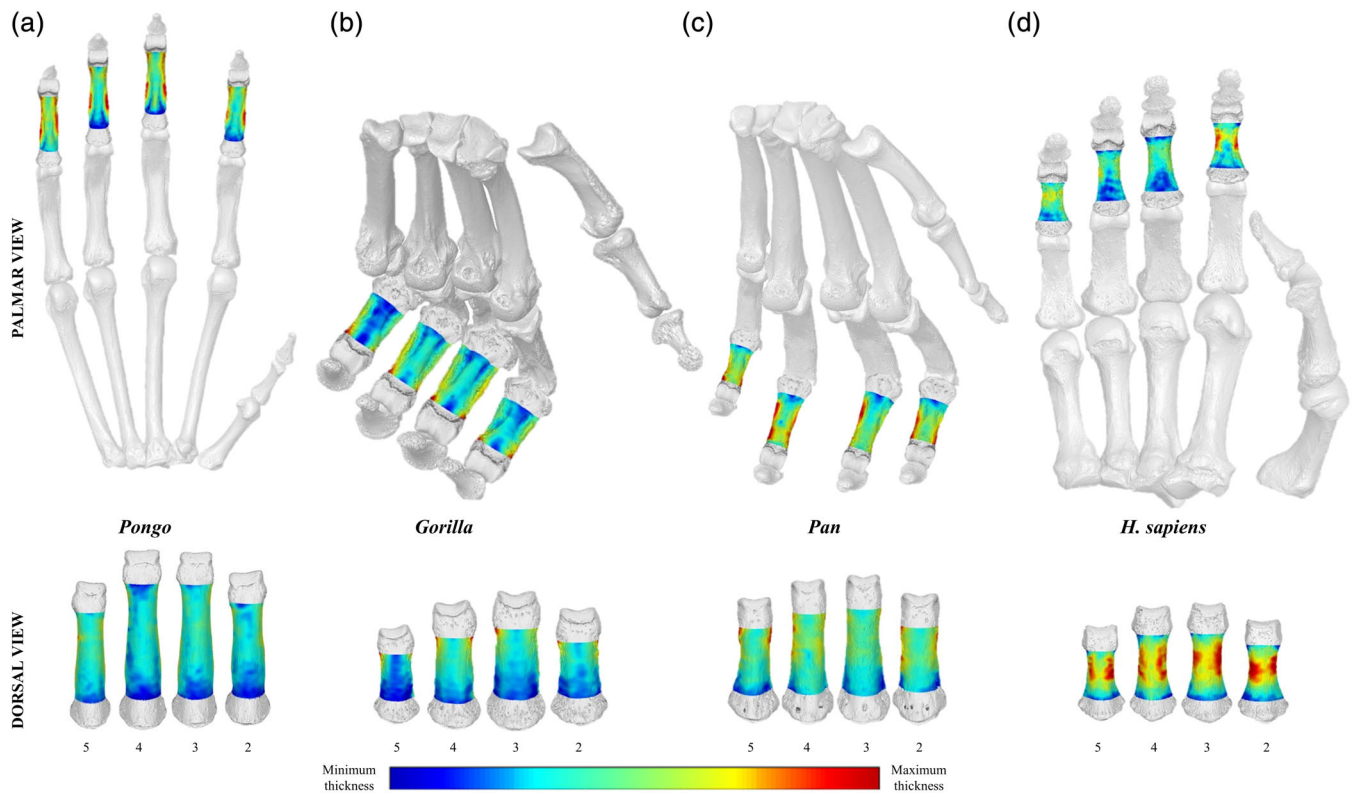


FIGURE 4 3D maps of cortical bone distribution across the intermediate phalanges in a representative individual of each taxon: (a) *Pongo pygmaeus*, (b) *Gorilla gorilla*, (c) *Pan troglodytes*, and (d) *Homo sapiens*. Thickness maps are independent of each other, and images are not to scale.

TABLE 2 Summary statistics of raw (mm) and standardized (dimensionless) cortical thickness measurements of the phalangeal shaft.

	<i>Homo sapiens</i>	<i>Pan</i>	<i>Gorilla</i>	<i>Pongo</i>
	Mean (SD)	Mean (SD)	Mean (SD)	Mean (SD)
Raw				
IP2	1.074 (0.300)	2.147 (0.289)	2.430 (0.361)	1.734 (0.240)
IP3	1.393 (0.383)	2.392 (0.342)	2.820 (0.387)	1.837 (0.300)
IP4	1.359 (0.387)	2.291 (0.293)	2.703 (0.457)	1.818 (0.250)
IP5	0.967 (0.264)	1.923 (0.346)	2.265 (0.428)	1.669 (0.300)
Standardized ^a				
IP2	0.042 (0.011)	0.068 (0.010)	0.070 (0.008)	0.047 (0.004)
IP3	0.047 (0.012)	0.058 (0.008)	0.067 (0.007)	0.042 (0.006)
IP4	0.046 (0.012)	0.061 (0.008)	0.068 (0.009)	0.041 (0.005)
IP5	0.046 (0.012)	0.070 (0.012)	0.073 (0.011)	0.046 (0.003)

^aStandardized by bone length.

3.1.1 | Cortical bone distribution patterns

Suspensory *Pongo* has thicker cortical bone on the peak of the FSRs and the region proximal to the trochlea, with the shaft ranging from

low to intermediate thickness relative to the regions of maximum thickness (Figure 4a). This pattern is generally similar across the four digits, with the exception of IP2 and IP5, where some individuals display cortical bone that is thicker on the ulnar FSR relative to the radial FSR (Figure 4a, Figure S1).

In knuckle-walking apes, thickest cortical bone is typically found from the FSRs up to the region proximal to the trochlea, while the cortical thickness of the shaft ranges from relatively low to intermediately thick (Figure 4b,c). However, compared to *Pan*, distribution of cortex of the *Gorilla* phalangeal shaft is generally low in thickness relative to its thick FSRs. Across *Gorilla* IP2–IP4, individuals that possess thick and prominent FSRs have a shaft relatively low in thickness, while individuals with relatively thinner and smaller FSRs have a shaft that is intermediate in its thickness (Figure 4b, Figure S1). In *Pan* individuals that do not possess prominent FSRs, only the region proximal to the trochlea is maximally thick while the remainder of the phalangeal shaft (including the FSRs) is relatively intermediate in its thickness (Figure 4c, Figure S1). Across the *Pan* hand, some individuals show thicker cortex radially in IP2 and IP3 compared to the ulnar surface.

The human pattern of cortical bone distribution is distinct from the other great apes, with the thickest cortical bone found on the dorsal midshaft-to-distal region as well as the disto-palmar region across the digits (Figure 4d, Figure S1). The FSRs, when present, are maximally thick as well.

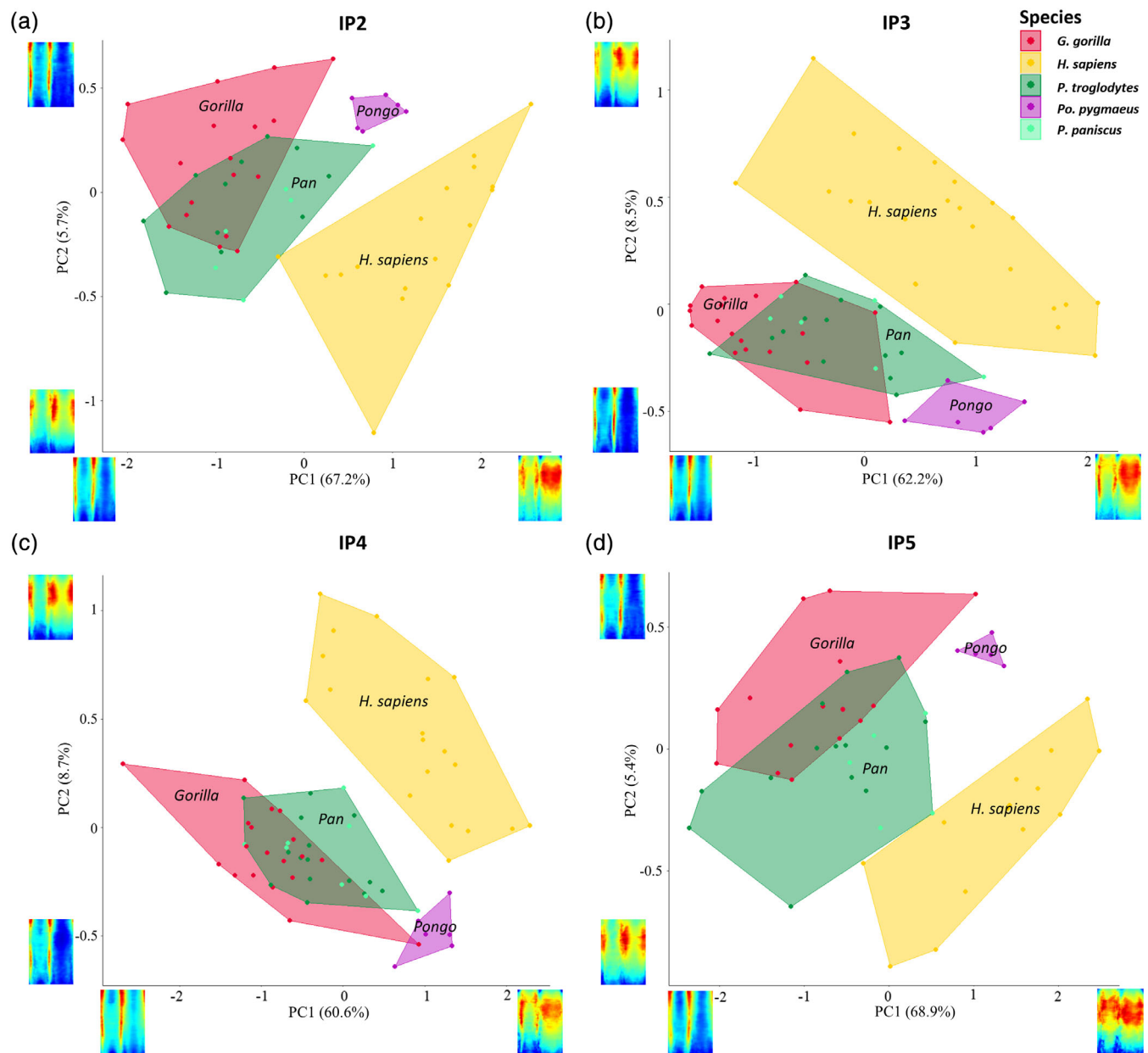


FIGURE 5 PC1 and PC2 for cortical bone distribution of intermediate phalanges of IP2, IP3, IP4, and IP5 of *Pongo*, *Gorilla*, *Pan* spp., and *Homo sapiens*.

3.1.2 | Cortical bone distribution variation across taxa

The PCA distinguishes taxa based on scaled cortical thickness distribution patterns of each phalanx. The results of the PCAs were similar between digits, with similar loadings and separation among the humans and non-human great apes (Figure 5; 3D PCA in Figure S2). PC1 explains between 60% and 69% of the total variance for each of the four digits. Low PC1 scores separate the African apes with relatively thicker FSRs and high PC1 scores distinguish humans with thicker cortex on the dorsal shaft along with thick radial and ulnar palmar cortex in IP2–IP4. IP5 distinguishes the species similarly, with the same loadings on low PC1 values, but high PC1 values represent thick midshaft-to-distal dorsal and palmar shaft thickness. African apes

variably overlap with each other, and *Pongo* is close to the humans and across all digits (Figure 5).

PC2 explains between 5% and 9% of the variance in the PCAs for each of the four digits and represents the region of overall maximum cortical thickness. Within IP2 and IP5, the nonhuman great apes are characterized by high PC2 scores, with maximum cortical thickness located on the palmar radial and ulnar surfaces, while humans have a wide range of PC2 scores with maximum cortical thickness located on the radial and ulnar surface of the mid-to-distal shaft. The PCA of IP3 and IP4 represents the same relative patterns, but the axes are flipped such that low PC2 scores generally characterize nonhuman great apes with thicker palmar radial and ulnar cortex and a wide range of PC2 values generally reflect humans having thicker cortical bone on the radial and ulnar surface of the mid-

TABLE 3 Significance values for post hoc comparisons of cortical thickness among species.

		<i>Pan</i>	<i>Gorilla</i>	<i>Pongo</i>
IP2	<i>Homo sapiens</i>	<0.001	<0.001	NS
	<i>Pan</i>		NS	0.021
	<i>Gorilla</i>			0.004
IP3	<i>Homo sapiens</i>	0.033	<0.001	NS
	<i>Pan</i>		NS	0.035
	<i>Gorilla</i>			<0.001
IP4	<i>Homo sapiens</i>	0.007	<0.001	NS
	<i>Pan</i>		NS	0.010
	<i>Gorilla</i>			<0.001
IP5	<i>Homo sapiens</i>	<0.001	<0.001	NS
	<i>Pan</i>		NS	0.034
	<i>Gorilla</i>			0.008

Note: The bold values are values that are statistically significant given a $p < 0.05$. Abbreviation: NS, not significant ($p > 0.05$).

to-distal shaft. Together, PC1 and PC2 generally separate humans from the other taxa in all rays.

3.1.3 | Mean cortical thickness

In interspecific comparisons, African apes have significantly thicker cortical bone than *Pongo* and *H. sapiens* across all digits (Table 3). No significant differences in cortical thickness were found between *Gorilla* and *Pan* or between *Pongo* and *Homo* in any digit. In comparisons of cortical thickness patterns across the hand, mean cortical thickness between the IPs does not significantly differ ($p > 0.05$) within *Pongo*, *Gorilla*, and *H. sapiens* (Figure S3). In contrast, in *Pan* mean cortical thickness of IP5 was significantly greater than that of IP3 and IP4, with mean cortical thickness of IP2 being significantly greater than IP3 as well (Figure S3).

3.1.4 | Mean cortical thickness across the shaft

Mean cortical thickness of the shaft reveals that all non-human great apes have a shared pattern across each of the four IPs (Figure 6). Mean cortical thickness increases up until the midshaft and from there remains consistent with the thickest cortex located at the distal end of the shaft. In contrast, in humans cortical thickness increases proximo-distally, peaking just distal to the midshaft and then decreases at the distal shaft in IP2–5.

3.1.5 | Palmar versus dorsal cortical thickness

A ratio of palmar and dorsal cortical thickness (Figure S4) reveals that within the *Pongo* digits, cortex on the palmar surface is significantly

thicker than the dorsal surface in all four digits except IP3 (Table 4). *Gorilla* and *Pan* have similar thickness values in the palmar and dorsal shaft, except in the *Gorilla* IP2 ($p = 0.033$) and *Pan* IP5 ($p = 0.045$) where the palmar cortex is significantly thicker. Across the human digits, the dorsal surface of the shaft has significantly thicker cortex than the palmar surface, with the exception of IP5 where there are no significant differences ($p > 0.05$).

3.2 | Cross sectional geometry

Descriptive statistics of the scaled cross-sectional geometric properties (CA, Z_{pol} , and J) at 35%, 50%, and 65% of the shaft are presented in Table S2 and depicted in Figures 7–9. There were differences across species in the different cross-sections in CA, Z_{pol} , and J for all four digits ($p < 0.05$), which are presented in Table S3.

In *Pongo*, CSG properties are similar in all cross-sections (35%, 50%, and 65%) (Figures 7–9), with no significant differences across IP2–IP5. Within *Gorilla*, IP3 is significantly greater than IP5 in all cross-sectional properties with some variation at the different cross-sectional levels (Table S4). At the 35% cross-section, there are no significant differences in CA across the *Gorilla* digits and at the 50% level, J of IP4 is also significantly greater than IP5. In *Pan*, the CSG properties across IP2–IP5 follow a similar pattern to that of *Gorilla*, with IP3 being significantly greater than IP5 in all CSG properties across the different cross-sections, with some variation in values of Z_{pol} and J at specific cross-sections (Table S4). In *H. sapiens* digits, only Z_{pol} of IP3 is significantly greater than IP5 and J of IP3 and IP4 greater than IP5 across all cross-sections (Table S4).

Analysis of intra-taxic differences in CSG properties at the different cross-sectional levels, reveal significant differences in CSG properties within the phalangeal shaft of *Gorilla*, *Pan*, and *H. sapiens* (Table S5). There are no significant differences across the *Pongo* digits. Within the *Gorilla* digits, CA at the midshaft of IP3 is significantly greater than at 65% of the shaft. Z_{pol} and J increase disto-proximally within the shaft, with values at the proximal end (35% of the shaft) being significantly greater than values at the distal end (65% of the shaft) in IP2–IP5 (Table S5). Within IP3, the values at the midshaft (50% of the shaft) are also significantly greater than values at the distal end (65% of the shaft). Mean values of all three CSG properties in *Pan* phalanges increase disto-proximally within the shaft (Table S2). In IP2–IP4, all CSG properties at the proximal end are significantly greater than the distal end the shaft, with values of Z_{pol} and J at the proximal end also being significantly greater than at the midshaft. Within IP5, only Z_{pol} and J at 35% of the shaft is greater than 65% of the shaft (Table S5). Within *H. sapiens*, CA is greatest at the midshaft and Z_{pol} and J increase disto-proximally, similar to *Pongo* and *Gorilla* (Figures 7–9; Table S2). There is little variation within the shaft of each digit such that only J at 35% of the shaft is greater than 65% of the shaft across IP2–4 and CA at 50% is significantly greater than 35% of the shaft only in IP2 (Table S5).

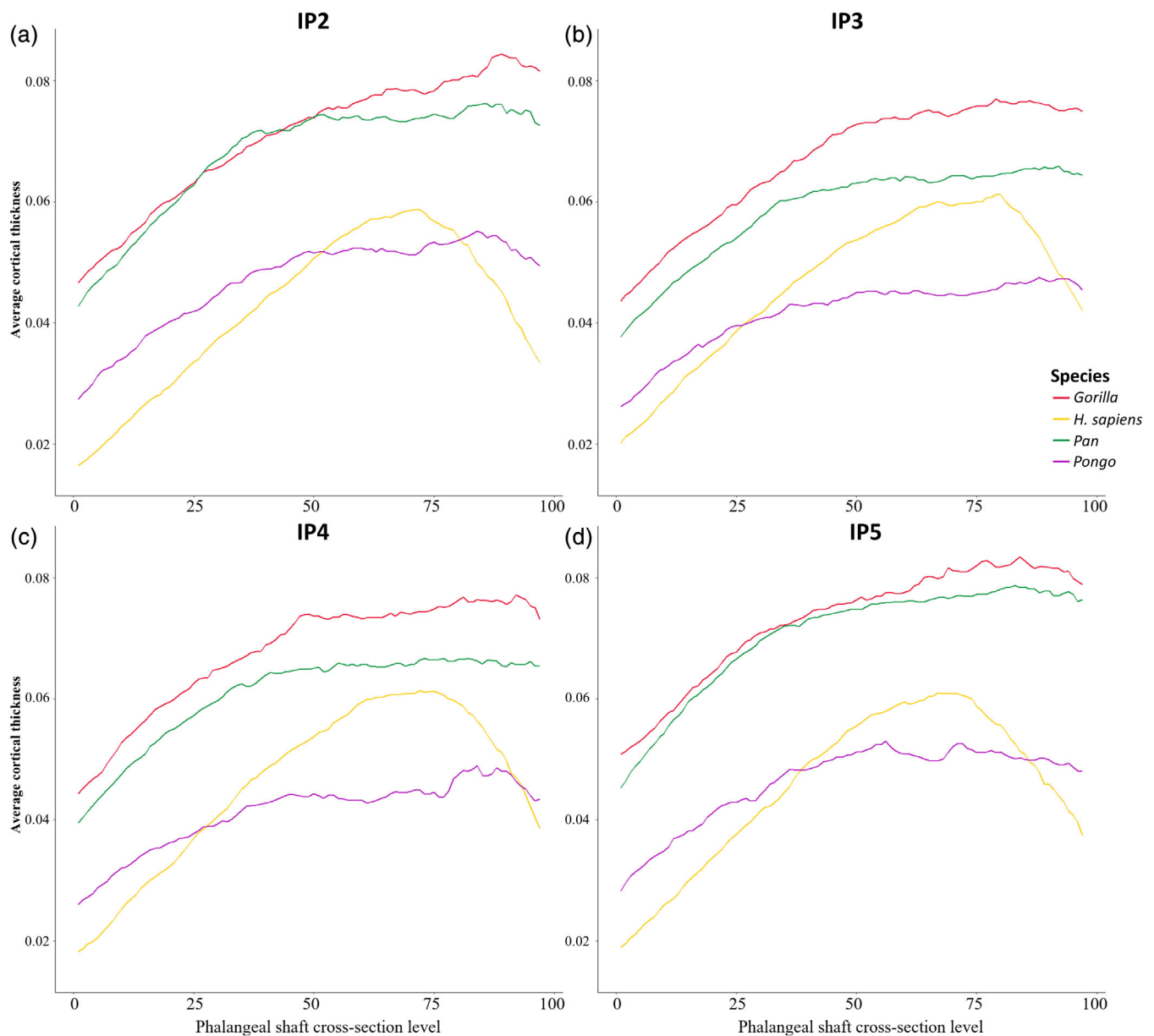


FIGURE 6 Average cortical bone thickness plotted from the proximal end (0) to the distal end (100) of the defined phalangeal shaft of *Pongo*, *Gorilla*, *Pan* spp., and *Homo sapiens*.

3.2.1 | Inter-taxic analysis of cross-sectional properties

Values of scaled cross-sectional properties are greatest in *Gorilla*, followed variably by *Pan* and *H. sapiens*, and are lowest in *Pongo* at the proximal end (35%) of the shaft. Distally (50% and 65% of the shaft) the pattern of CA is similar, but Z_{pol} and J is greatest in *Gorilla*, followed by *H. sapiens*, *Pan*, and *Pongo* (Table S2). Significance tests reveal *Gorilla* has significantly larger values of CA, Z_{pol} , and J across all digits and cross-sectional levels compared to the other taxa, except for Z_{pol} and J in IP5 at 50% cross-section (Table S3). At the 50% level in IP5, *Gorilla* is only greater than *Pan* in Z_{pol} and greater than *Pan* and *H. sapiens* in J . Overall, the remaining taxa, *Pongo*, *Pan*, and *H. sapiens*

are not significantly different from each other in any cross-sectional properties across the different levels, except for CA. Values of CA in the IP2 of *Pan* are significantly greater than that of *H. sapiens* at 35% of the shaft.

3.3 | Cortical thickness and external morphology

3.3.1 | Phalangeal curvature and cortical thickness

Regression analyses testing the relationship between phalangeal cortical thickness and curvature across the extant great apes reveal that there is no relationship between the cortical thickness and degree of

TABLE 4 Paired samples *t*-tests palmar versus dorsal thickness across species.

		<i>Homo sapiens</i>	<i>Pan</i>	<i>Gorilla</i>	<i>Pongo</i>
IP2	Palmar mean	0.035	0.061	0.062	0.046
	Dorsal mean	0.045	0.058	0.058	0.039
	<i>t</i> -ratio	-3.328	1.522	2.170	4.061
	<i>p</i>	<0.001	NS	0.033	<0.001
IP3	Palmar mean	0.037	0.053	0.057	0.040
	Dorsal mean	0.050	0.051	0.057	0.036
	<i>t</i> -ratio	-5.634	0.861	-0.222	2.021
	<i>p</i>	<0.001	NS	NS	NS
IP4	Palmar mean	0.036	0.056	0.058	0.041
	Dorsal mean	0.049	0.053	0.058	0.035
	<i>t</i> -ratio	-5.038	1.531	-0.016	2.757
	<i>p</i>	<0.001	NS	NS	0.013
IP5	Palmar mean	0.042	0.066	0.064	0.046
	Dorsal mean	0.047	0.062	0.062	0.038
	<i>t</i> -ratio	-1.689	2.036	1.158	4.992
	<i>p</i>	NS	0.045	NS	<0.001

Abbreviation: NS, not significant ($p > 0.05$). The bold values in are values that are statistically significant given a $p < 0.05$.

curvature of the intermediate phalanges of *Pan*, IP2 and IP4–IP5 of *Pongo*, IP2–IP4 of *Gorilla*, and IP3–IP5 of humans (Figure S5; Table S6). There is a significant but weak relationship between the curvature and cortical thickness of *Pongo* IP3 ($p = 0.030$ and $R^2 = 0.073$), *Gorilla* IP5 ($p = 0.022$ and $R^2 = 0.321$), and *H. sapiens* IP2 ($p = 0.024$ and $R^2 = 0.295$) (Table S6).

3.3.2 | Palmar surface morphology and cortical thickness

Testing the relationship between phalangeal cortical thickness, median bar height, FSR length, and FSR depth in the IP3 of our sample reveals weak but significant relationships between these variables in *Gorilla*, *Pan*, and *H. sapiens* (Tables S7–S9 and S11). Within these variables, there is no significant relationship between FSR length of median bar of extant hominid IP3s (Table S10).

3.4 | Comparison of proximal and intermediate phalanges

3.4.1 | Mean cortical thickness

Comparing scaled mean cortical thickness values in the proximal and intermediate phalanges of digits 2–5, cortical thickness values of the intermediate phalanges are significantly greater than the proximal phalanges across all taxa (Figure 10). However, the raw values reveal a different pattern for each species (Figure 11). In *Pongo*, there are no

significant differences between the raw cortical thickness of the proximal and intermediate phalanges. Within knuckle-walkers, *Gorilla* cortical thickness of the proximal phalanges is greater in digit 2 and 3, while in *Pan* all proximal phalanges have significantly thicker cortex than the associated intermediate phalanges. In humans, there are no significant differences across the digits except for digit 2 in which the cortical thickness of the proximal phalanx is significantly greater than that of its associated intermediate phalanx.

3.4.2 | Cross-sectional geometry

Analyzing relative CSG properties between the proximal and intermediate phalanges of digits 2–5 reveals greater variation in the mean values of Z_{pol} and J compared to CA. Across the digits and three cross-sections, there are no significant differences in the mean values of CA between the proximal and intermediate phalanges of *Pongo*, *Gorilla*, and *H. sapiens* (Table S12). *Pan* has significantly greater values of CA in the proximal phalanges of digits 2–4 at 35% and 65% of the shaft.

Mean values of Z_{pol} in *Pongo* are significantly greater in the proximal phalanx of digit 2 at 35% and 65% of the shaft ($p = 0.036$ and $p = 0.033$, respectively), and in the proximal phalanx of digit 3 at 50% and 65% of the shaft ($p = 0.035$ and $p = 0.003$, respectively) (Table S13). Within the proximal and intermediate phalanges of *Gorilla*, Z_{pol} values are significantly greater in the proximal phalanges across all digits and cross-sections. Mean Z_{pol} values of *Pan* are significantly greater in the proximal phalanges of digit 3 and 4 at 35% of the shaft, digit 2–4 at 50% of the shaft, and across all digits at 65% of the shaft (Table S13). Within the human proximal and intermediate phalanges, the proximal phalanx of digit 2 has significantly greater values than the intermediate phalanx at 35% and 50% of the shaft and across digits 2–4 at 65% of the shaft.

Across the digits of *Pongo*, relative mean values of J are greater in the proximal phalanx of digit 3 at 50% of the shaft and across digit 2–4 at 65% of the shaft (Table S14). Similar to the Z_{pol} values of *Gorilla*, mean values of J are significantly greater in the proximal phalanges of all four digits across all three cross-sections. Within the proximal and intermediate phalanges of *Pan*, the proximal phalanx of digit 4 has significantly greater values of J than the intermediate phalanx at 35% of the shaft. At 50% and 65% of the shaft, the proximal phalanges of all four digits have significantly greater values of J compared to the intermediate phalanges. The human proximal phalanges have significantly greater values of J for: digit 2 at 35% of the shaft, digit 2 and 3 at 50% of the shaft, and digit 2–4 at 65% of the shaft.

4 | DISCUSSION

Studies of internal structure of the hand have generally focused on the metacarpus and elements of the carpus, with the phalanges being comparatively understudied (e.g., Bird et al., 2022; Dunmore et al., 2019; Marchi, 2005; Skinner et al., 2015). Here, we investigated

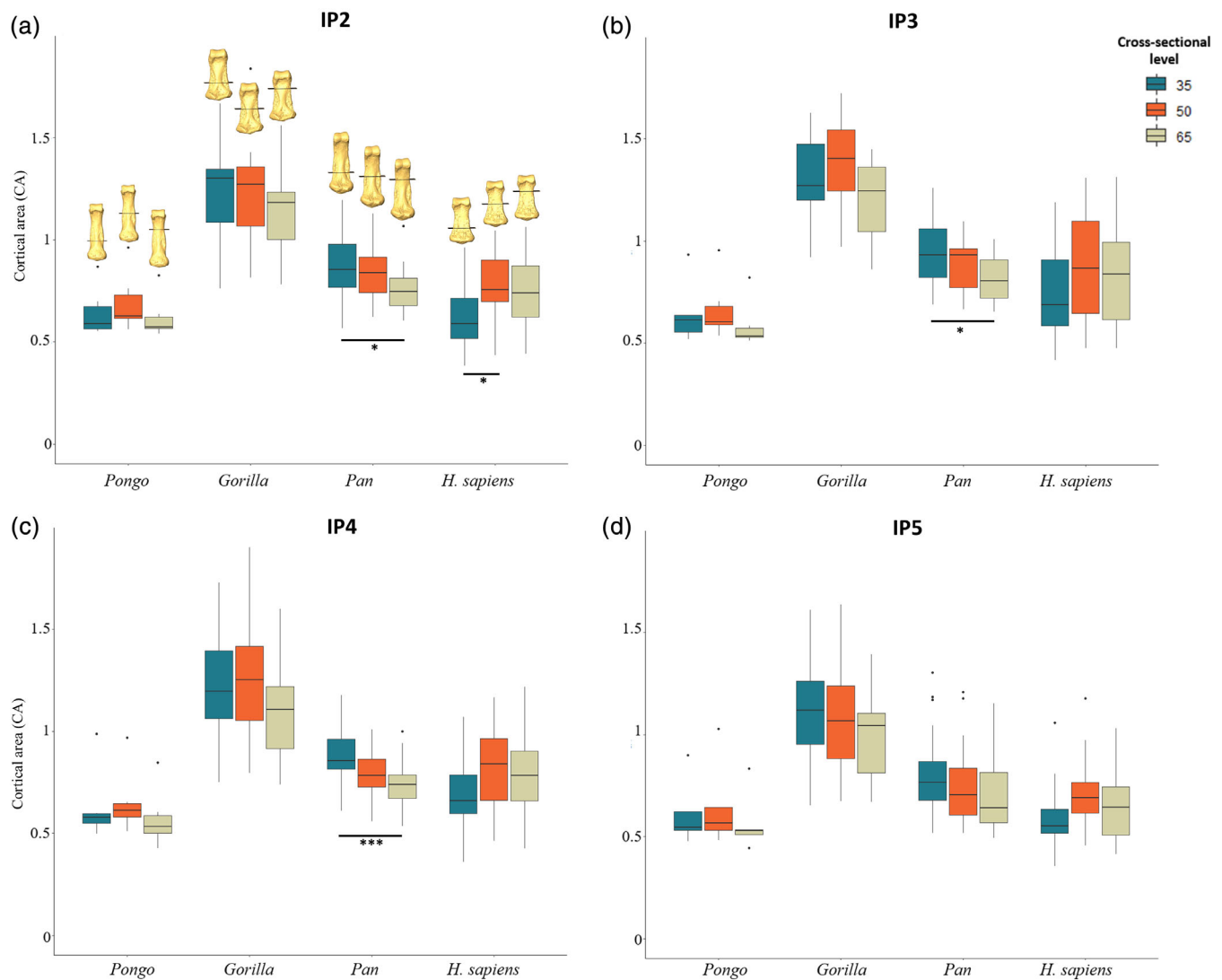


FIGURE 7 Cortical area (CA) for digits 2–5 of *Pongo*, *Gorilla*, *Pan* spp., and *Homo sapiens* at 35%, 50%, and 65% of the bone length. * $p < 0.05$; ** $p < 0.01$; *** $p < 0.001$.

variation in hominoid cortical bone distribution patterns of the intermediate phalanges of digits 2–5 in relation to hand use and postures, building upon our previous study of proximal phalanges in the same taxa (and specimens) (Syeda et al., 2023). Cortical bone distribution patterns, along with overall cortical bone thickness and CSG properties, were consistent with differences in hand use among suspensory *Pongo*, knuckle-walking *Gorilla* and *Pan*, and humans. Comparisons of cortical bone structure between the proximal and intermediate phalanges, provides greater insight into digit loading during manual behaviors.

4.1 | Extant great ape intermediate phalangeal cortical distribution, thickness and cortical properties

We predicted that cortical bone in *Pongo* would be thickest in the midshaft-to-distal palmar surfaces with no significant differences in

cortical structure across the digits, reflecting the flexed-finger, hook grip of all the fingers during suspensory behaviors (Rose, 1988; Sarmiento, 1988). Our predictions were supported. In *Pongo* regions of thickest cortical bone were located proximally on the FSRs and in the region proximal to the trochlea, with the remaining shaft having low to intermediate thickness across all IPs. This pattern reflects the known biomechanical role of the FSRs and phalangeal curvature, which is to reduce strain on the phalangeal shaft (Nguyen et al., 2014; Richmond, 2007). The lack of significant differences in cortical thickness and CSG properties across the digits is consistent with equal use and similar loading of all four digits during suspensory locomotion in *Pongo* (Rose, 1988; Susman, 1974; Thorpe & Crompton, 2006).

Within the African apes, we predicted that *Gorilla* and *Pan* would have a similar pattern of cortical bone distribution but would differ in their cortical bone properties across the digits. Our predictions were not fully supported. The general African ape pattern across the rays was characterized by thick cortical bone at the FSRs and proximal to

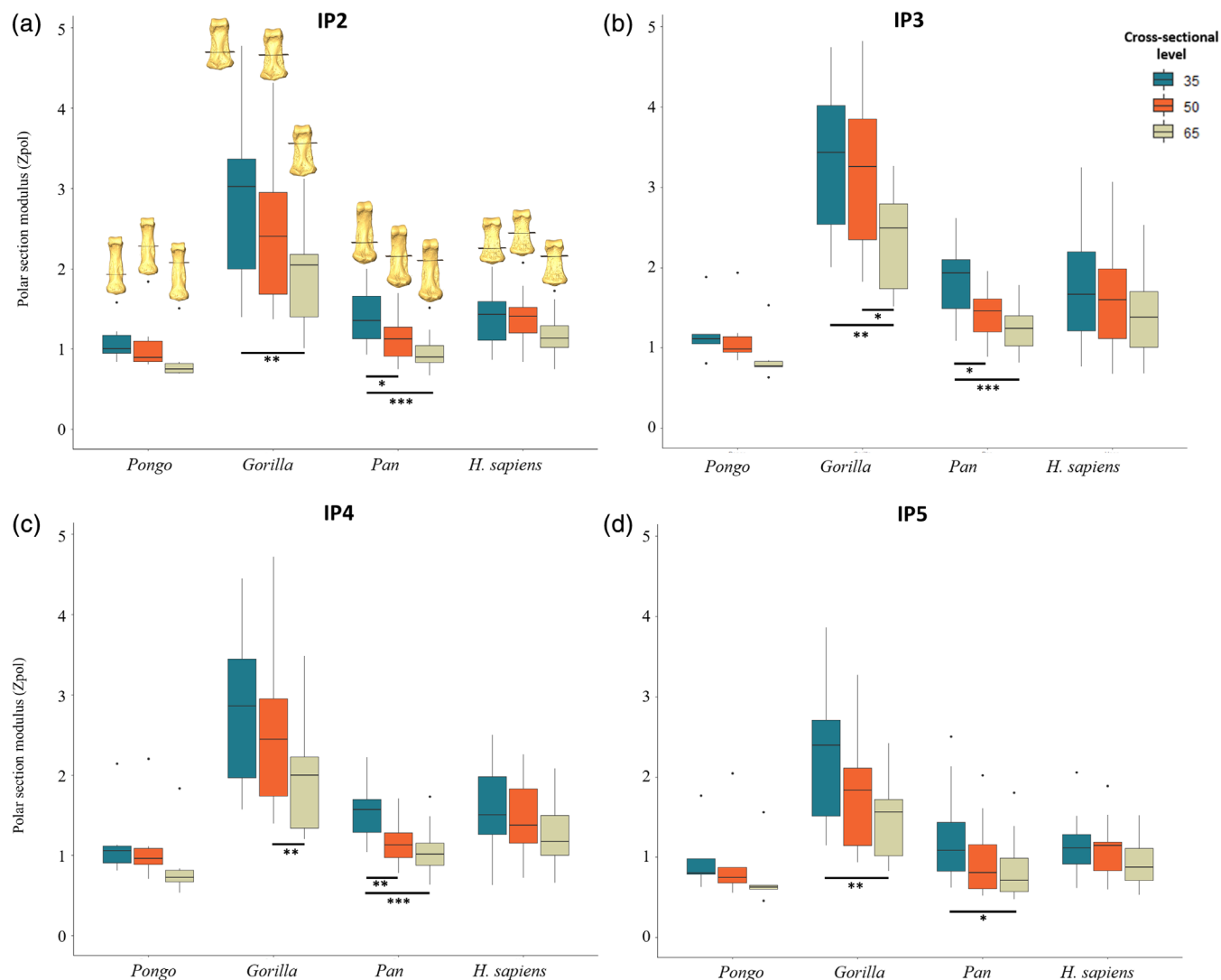


FIGURE 8 Polar section modulus (Z_{pol}) for digits 2–5 of *Pongo*, *Gorilla*, *Pan* spp., and *Homo sapiens* at 35%, 50%, and 65% of the bone length. * $p < 0.05$; ** $p < 0.01$; *** $p < 0.001$.

the trochlea, with a low to intermediately thick cortex along the shaft. This African ape pattern differs from *Pongo* in that the African ape FSRs generally span the majority of the proximodistal length of the phalanx, while in *Pongo* the FSRs are located on the proximal half of the shaft. The African ape pattern is surprising as EMG data on sub-adult chimpanzees has shown minimal to no activation of flexor muscles during knuckle-walking (Susman & Stern, 1979). However, a recent experimental study has shown stress is concentrated on pulleys, which hold the flexor tendon close to the bone during interphalangeal joint flexion (Leijnse et al., 2021). These pulleys arise from the radial and ulnar edges of the palmar surface, with annular pulleys A2 and A4 being the main pulleys within the fingers (Ayhan & Ayhan, 2020). The A4 pulley is located on the intermediate phalanges and Leijnse et al. (2021) have shown that stress is concentrated proximally on the A4 pulley, which coincides with the location of the FSRs. Although Marzke et al. (2007) found no relationship between the size of the FDS tendon and palmar phalangeal morphology, if the regions

of thickest cortex reflect stress related to the adjacent A4 pulley insertions, then cortical bone distribution patterns may be reflecting the role of the flexor muscles during different African ape manual behaviors that are not reflected in external morphology alone. These manual behaviors could include stretching of the flexor tendons during knuckle-walking (Leijnse et al., 2021) or activation of flexor muscles during arboreal grasping (Susman & Stern, 1979). While the overall pattern is generally similar, the majority (82%) of *Pan* individuals had an intermediately thick shaft while the majority (69%) of *Gorilla* individuals had a relatively thin shaft cortex. This difference may reflect the greater frequency of arboreal behaviors in *Pan* and thus flexor muscle activation, as well as differences in the external morphology (Hunt, 2020; Susman, 1979; Susman & Stern, 1979). *Gorilla* has a significantly lower degree of phalangeal curvature than *Pan*, while *Pan* has significantly smaller FSRs than *Gorilla* (Doran, 1996; Hunt, 1992; Sarringhaus et al., 2014; Susman, 1979; Syeda et al., 2021).

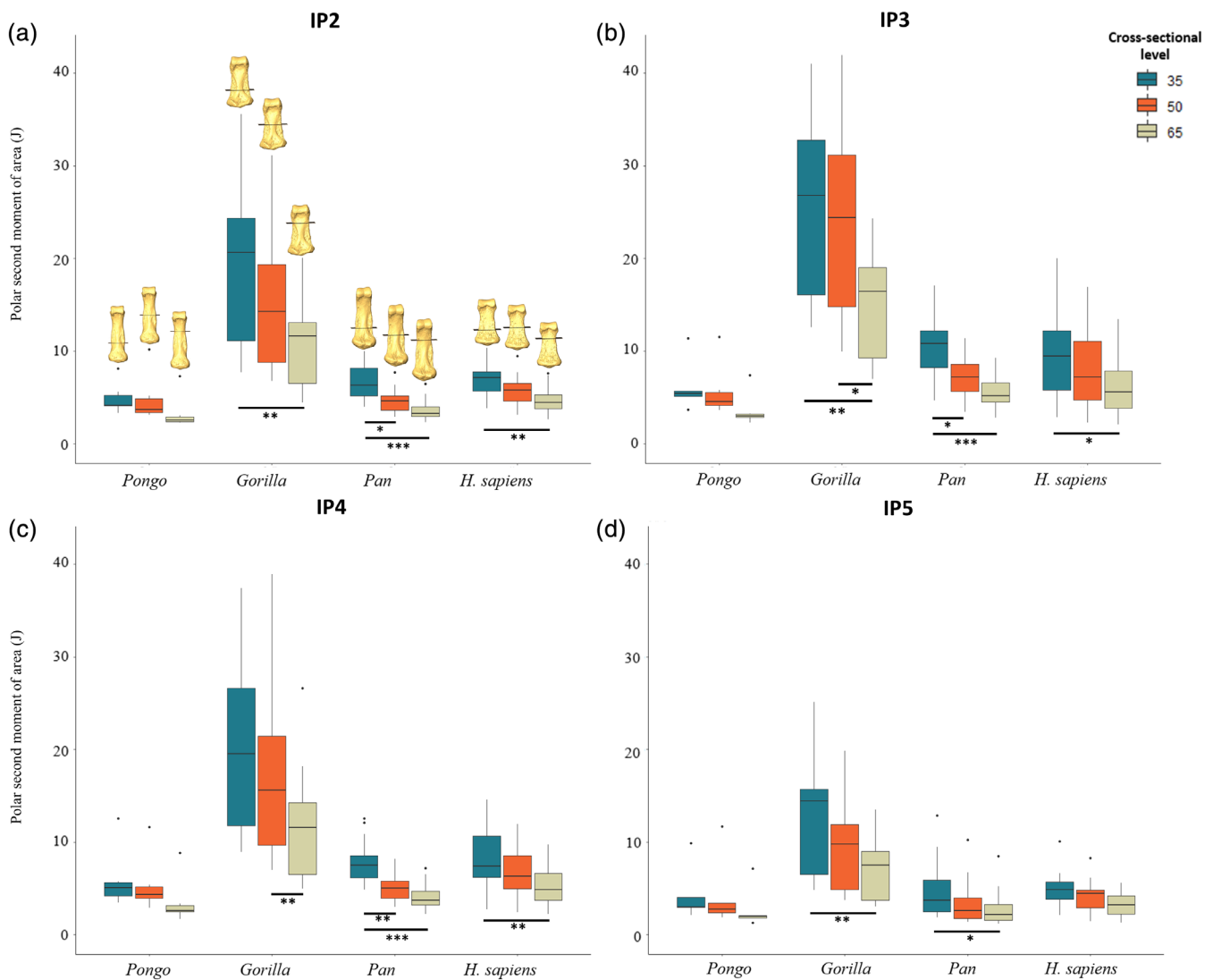


FIGURE 9 Polar second moment of area (J) for digits 2–5 of *Pongo*, *Gorilla*, *Pan* spp., and *H. sapiens* at 35%, 50%, and 65% of the bone length. * $p < 0.05$; ** $p < 0.01$; *** $p < 0.001$.

Along with differences in cortical bone distribution pattern between the African apes, cortical properties of the intermediate phalanges across the digits differ between *Gorilla* and *Pan*. This result is consistent with data from captive individuals showing differences in digit use and loading between these two taxa (Matarazzo, 2013; Samuel et al., 2018; Thompson, 2020; Wunderlich & Jungers, 2009). While recent observations of mountain gorillas in the wild show much greater variation in manual postures than in captivity (Thompson et al., 2018), zoo-housed *Gorilla* loads digits 2–5 more evenly than *Pan* (Matarazzo, 2013; Tuttle, 1969). This is reflected in the variation in cortical properties across the digits of the respective taxa. *Gorilla* mean cortical thickness does not significantly differ across the digits but CSG properties show that IP3 is significantly stronger than IP5, which is consistent with pressure studies that have shown greater loads occurring around the midline of the hand during knuckle-walking (Samuel et al., 2018; Tuttle et al., 1972). Contrary to our prediction, IP5 of *Pan* had significantly thicker cortical bone than IP3 and IP4, which are the digits that experience the highest loading

(Matarazzo, 2013; Samuel et al., 2018; Wunderlich & Jungers, 2009). However, the *Pan* IP3 did have CSG properties reflecting greater strength relative to IP5. The thicker cortex and weaker CSG properties of IP5 relative to IP3 may reflect the role of external morphological features in the modeling of internal bone structure. IP5 has smaller FSRs and a lower degree of phalangeal curvature (Susman, 1979; Syeda et al., 2021) that, all things being equal, would increase strain experienced by the shaft on the IP5 relative to the IP3 (Nguyen et al., 2014).

As predicted, human cortical bone was thickest on the distodorsal region, including in individuals that possess well-developed FSRs. This cortical bone distribution pattern may reflect the role of phalangeal curvature in dissipating forces across the phalanx. Typically, *H. sapiens* manual behaviors involve flexed-finger postures in which the dorsal surfaces of the phalanges experience high compressive forces and the palmar surfaces experience tensile forces. These bending forces dissipated across a relatively straight phalanx result in greater stress experienced by the dorsal surface (Preuschoft, 1973). Along with thick

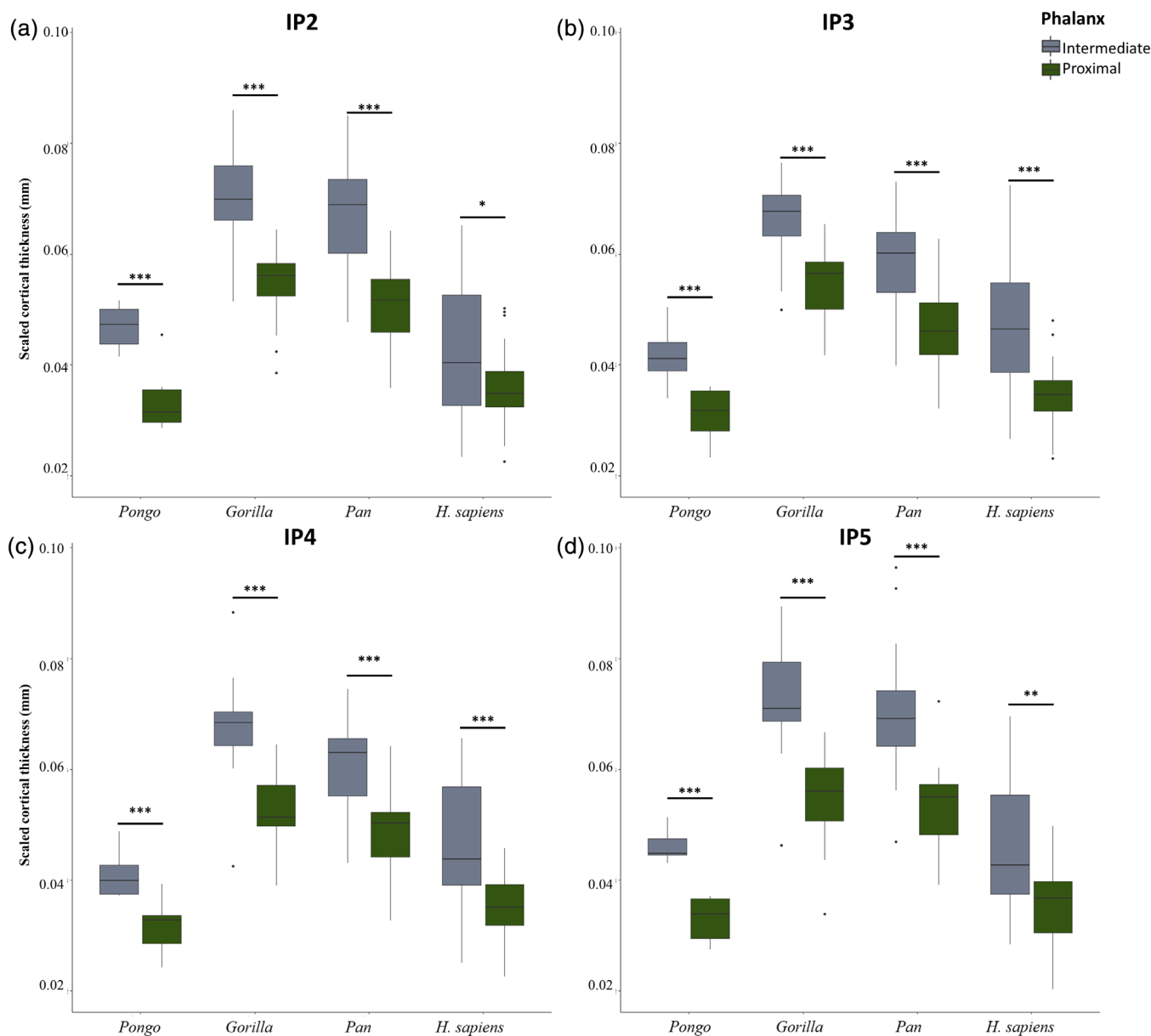


FIGURE 10 Scaled cortical thickness of the proximal and intermediate phalanges across (a) IP2; (b) IP3; (c) IP4; (d) IP5 of *Pongo*, *Gorilla*, *Pan* spp., and *Homo sapiens*. * $p < 0.05$; ** $p < 0.01$; *** $p < 0.001$. Intermediate phalanges have significantly thicker cortex in all taxa across the digits.

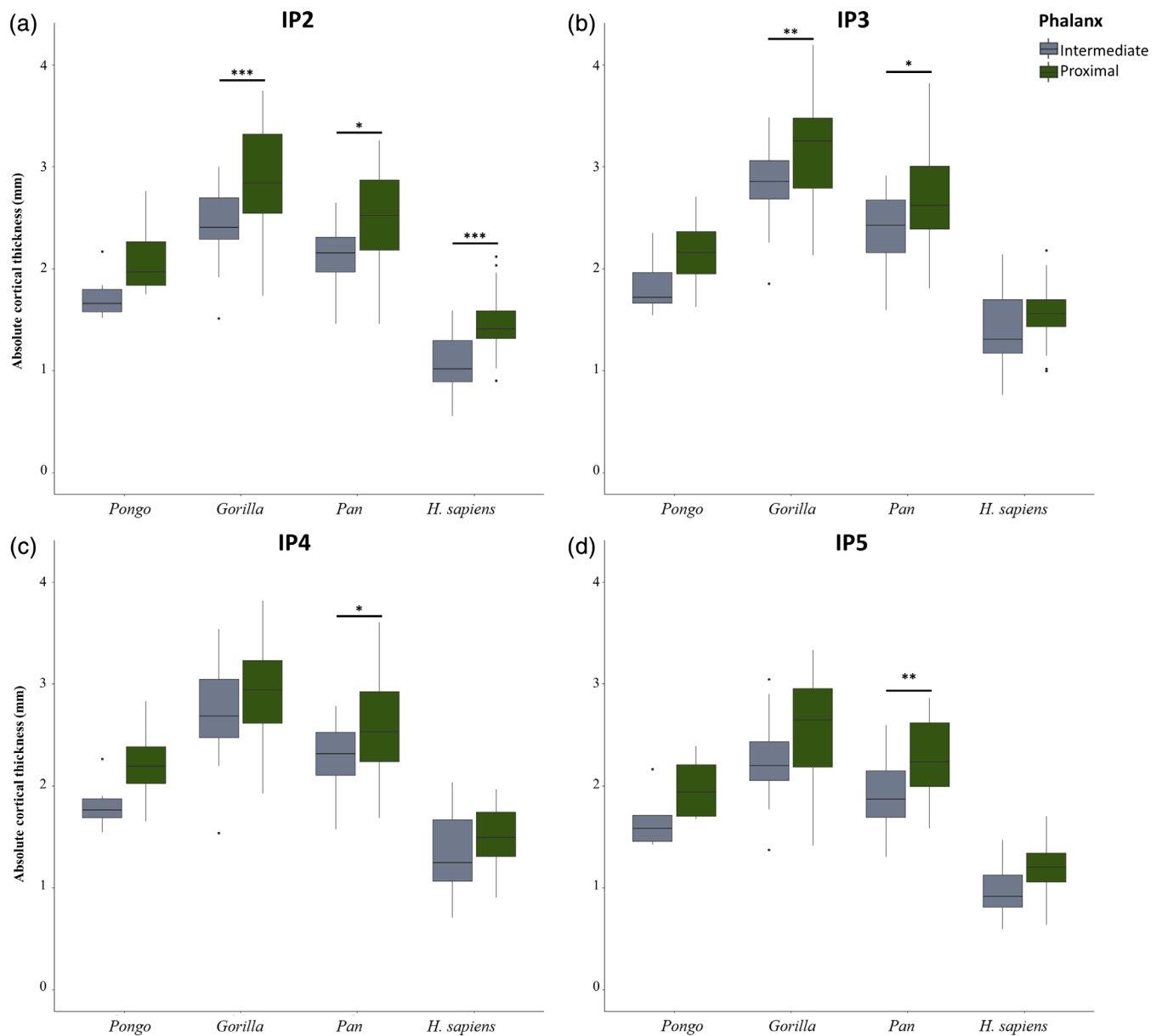
distodorsal cortex in humans, cortical bone on the distal palmo-radial and palmo-ulnar surfaces is thick irrespective of the presence of FSRs (Figure S1). In contrast, human proximal phalanges did not show consistently thick cortex at the radial and ulnar edges of the palmar surface (Syeda et al., 2023), suggesting that the pattern found in human IPs reflects the point of insertion of the FDS tendon. Across the hand, we predicted that digits 2 and 3 would have thicker cortices and stronger cortical properties than digits 4 and 5 as experimental studies have shown that greatest loads are experienced by the radial digits and the thumb (Cepriá-Bernal et al., 2017; De Monsabert et al., 2012; Sancho-Bru et al., 2014). However, our prediction is not supported; only IP3 was higher than IP5 in measures of bending strength (Z_{pol}) and only IP3 and IP4 were higher than IP5 in measures of bending

and torsional rigidity (J). The lack of distinct differences across the digits may reflect the presumed varied manual behaviors employed by our *H. sapiens* sample, which ranges from fossil specimens to a diverse range of pre- and post-industrial populations.

4.2 | Intermediate phalangeal pattern of cortical bone distribution compared to proximal phalanges

4.2.1 | *Pongo*

This cortical bone distribution pattern of *Pongo* IPs is similar to that of their PPs, further reflecting similar loading across the digits during



flexed-fingered grips of the hand. It is an oversimplification to classify *Pongo* hand postural behaviors to just hook-like grips, as variation in *Pongo* locomotion and hand use has been increasingly observed (McClure et al., 2012; Thorpe & Crompton, 2006). However, we expect phalangeal cortical structure to reflect the repetitive hand postural behaviors of *Pongo*, which have generally been observed to be flexed-fingered grips (Napier, 1960; Rose, 1988). While the proximal and intermediate phalanges share a general pattern of thickness localized at the FSRs with an intermediately thick shaft, there is a slightly different pattern observed in PP2. The PP2 of some individuals showed thicker palmar radial cortex (Syeda et al., 2023), which was hypothesized to reflect greater extension of the second digit when

grasping thin substrates (Napier, 1960). However, if this hypothesis is correct, we would expect a similar cortical distribution on the IP2, which we did not find. Instead, our sample of IP2s has relatively thicker cortex on the ulnar, rather than radial, edge of the palmar surface in most individuals. However, our sample of intermediate phalanges is constrained to only six individuals and thus these patterns may reflect general variation within this taxon. Deducing more subtle differences in hand postures will require larger sample sizes and detailed observational, and ideally biomechanical, data on hand use during *Pongo* locomotion.

Comparing cortical thickness values and cross-sectional properties of *Pongo* intermediate and proximal phalanges revealed mixed

signals. Scaled average cortical thickness of the IPs was significantly greater than the PPs across all digits. However, bending strength of PP2 and PP3 was significantly higher than their IPs and the bending and torsional rigidity of digit 2–4 PPs was significantly greater than the IPs in the distal region of the shaft (65% cross-section). While the IPs had thicker cortices than the PPs on average, higher CSG values of the PPs relative to the IPs could reflect the disto-proximal increase in load across the digit (Cooney & Chao, 1977), such that the PPs are experiencing greater forces and are better structurally adapted to resist greater loads (Matarazzo, 2015).

4.2.2 | Gorilla

Similar to the pattern previously identified in the *Gorilla* PPs (Syeda et al., 2023), the regions of thickest cortical bone in the IPs coincides with attachment points of soft tissues that stabilize the interphalangeal joints. Cortical bone of the PPs was thickest in patches along the FSRs, while in the IPs thick cortical bone was found across the length of the FSRs. The FSRs of the IPs are located on the proximal half of the phalangeal shaft, and as stress is concentrated proximally at the A4 annular pulley (Leijnse et al., 2021), this thickness of the FSRs in the proximal region of the bone may reflect the stress that occurs when the FDS tendon is bent during knuckle-walking. Similarly, the cortical bone distribution pattern of the PPs may reflect FDS tendon bending that occurs distally at the A2 annular pulley. These similar patterns of thick cortical bone in regions that are thought to be stressed by FDS tendon stretching and phalangeal soft tissue attachment points may provide support for experimental evidence that suggests that, during knuckle-walking, stress is concentrated at the maximum bending point of the tendons and at the pulleys which hold these tendons close to the shaft (Leijnse et al., 2021). Alternatively, these patterns might be a signal of less frequent (relative to knuckle-walking) arboreal behaviors (Hunt, 2020) in which the flexor muscles are highly active (Susman & Stern, 1979).

Across the PPs and IPs of *Gorilla* digits 2–5, the average scaled IP cortical thickness was significantly thicker than the PPs. Along with their thick cortices, there was also greater variation within the CSG properties across phalangeal shaft in the IPs compared to that of the PPs, such that the CSG properties at the proximal end of the bone were significantly greater than at the distal end. However, bending strength and resistance to bending and torsional rigidity is significantly greater in the PPs relative to the IPs. These results could indicate that despite the IPs making the initial contact with the substrate and directly incurring the ground reaction forces during knuckle-walking, the proximal end of the IPs and the PPs, as a whole, are better able to resist the forces generated during manual behaviors. Across the PPs and IPs, digit 2 shows thicker palmar cortex, which may reflect the relatively small FSRs of digit 2 compared to digits 3 and 4 (Susman, 1979), however it does not explain why PP5 has relatively thicker palmar cortex but IP5 does not.

4.2.3 | Pan

The pattern of cortical bone distribution of *Pan* IPs was similar to that reported for the PPs (Syeda et al., 2023), in that the region of thickest cortical bone was located proximodistally along the FSRs. Across our sample, *Pan* was the only taxon that showed differences in mean cortical thickness across the digits within its PPs and IPs. The proximal and intermediate phalanx of digit 5 had significantly thicker cortical bone than the proximal and intermediate phalanx of digit 3. However, the CSG properties of digit 3 were significantly greater than digit 5. This may be because the external morphological features of digit 5 (i.e., tall FSRs, phalangeal curvature) are not as prominent as they are in the other radial digits. Thus, loads may not be dissipated as effectively in digit five, leading to higher strains experienced by the shaft, increased cortical bone modeling and thus thicker cortical bone compared with digit 3, in which external morphological features are most pronounced (Nguyen et al., 2014; Susman, 1979). Average cortical thickness was greater in the IPs while the PPs had significantly stronger CSG properties than the IPs; a pattern similar to that found in *Gorilla*. As the primary mode of locomotion of *Gorilla* and *Pan* is knuckle-walking, these similarities in cortical bone structure of the PPs and IPs are expected.

4.2.4 | Homo sapiens

The cortical bone pattern of *H. sapiens* IPs was similar to that found in their PPs (Syeda et al., 2023) in that the thickest region of cortical bone was concentrated at the distodorsal surface of the phalanges. However, the IPs were distinct in also having thick cortical bone along the distodorsal region of the palmar surface (regardless of the development of the FSRs). There were no significant differences in cortical thickness across the digits in either the PPs or the IPs and the dorsal cortex was consistently thicker than the palmar cortex, except for in IP5. In IP5, similar dorsal and palmar cortical thickness may indicate that IP5 is not being loaded in the same manner as the other phalanges. This has been noted in an experimental study of load distribution during power grips, in which the fifth digit does not remain active throughout the length of a gripping task in contrast to the remaining digits (Sancho-Bru et al., 2014). This is also reflected in the CSG properties of the PPs and IPs, with CSG properties in the PPs of digits 2–4—but not digit 5—being significantly stronger than the IPs. The absence of differences in the CSG properties of the phalanges of digit 5 may reflect overall lower levels of loading for this digit.

4.3 | Relationship between proximal and intermediate cortical bone thickness

While the pattern of cortical bone distribution was similar in the proximal and intermediate phalanges within our study taxa, the scaled values of mean cortical thickness were not. Intermediate phalanges on

average had thicker cortical bone in the phalangeal shaft when scaled to the length of the bone. This could be due to many factors. First, external morphological features that are thought to help resist forces are generally less developed in the IPs compared to the PPs (i.e., degree of curvature; development of FSRs). Therefore, the relative cortical thickness in the intermediate phalanges may need to be greater to withstand higher bone strain experienced by the shaft. Second, the FDS tendons insertion site is located on the intermediate phalanges, whereas they are only passing across the proximal phalanx (with pulleys inhibiting the buckling of the tendon). Therefore, the majority of the internal forces exerted by these muscular tendons are likely incurred by the intermediate phalanges. Finally, it could be that the relationship between bone length and required cortical thickness is not linear such the minimum amount of cortical bone needed when scaled for length is larger than that required for longer proximal phalanges.

Comparing absolute values of PP and IP cortical thickness reveals a unique relationship between the two in each taxon (Figures 10 and 11). Similar values of absolute average cortical thickness across the PPs and IPs of *Pongo*, coupled with their thin cortex and low cross-sectional properties, may further reflect that, due to their external morphology minimizing strain on the phalangeal shaft, cortical modeling and thicker cortex might not be needed (Ruff et al., 2006; Syeda et al., 2023). Within the African apes, *Gorilla* had significantly thicker cortical bone in the PP of digits 2 and 3 while *Pan* had significantly thicker PP cortical structure across all digits. These results provide additional support for our inference that the PPs of African apes might be better adapted to the loads resulting from their manual behaviors compared to their IPs. Across *H. sapiens* digits, only digit 2 had significantly thicker cortical bone in the PP relative to the IP, while the remaining digits showed no differences. The absolutely thicker cortices of the PPs can be attributed to the absolutely larger size compared to the IPs, but the general lack of significant differences in PP and IP absolute cortical thickness of *Pongo*, *Gorilla*, and *H. sapiens* digits indicates phalangeal size is not the only factor impacting phalangeal cortical thickness.

4.4 | Phalangeal curvature

We found significant, but not strong, correlations between cortical thickness and the degree of curvature in the IPs and PPs (Syeda et al., 2023) in our sample. These results might therefore call into question the functional significance or plasticity of phalangeal curvature (see also Wallace et al., 2020). Phalangeal curvature has been shown to change throughout ontogeny based on the frequency of arboreality (Richmond, 1998) and has been experimentally demonstrated to reduce strain experienced by the (proximal) phalanx during suspensory loading (Nguyen et al., 2014; Richmond, 2007). If cortical thickness reflects loads incurred during life (Ruff et al., 2006), one might expect taxa with more curved phalanges to have thinner cortex or for humans to have more curved phalanges if they are habitually using flexed-finger postures. However, our results suggest that the

relationship between cortical bone thickness and curvature is more complex. Overall length of the phalanx and the shape and size of the flexor sheath ridges will also influence how loads are incurred by the phalanx, and the frequency and magnitude of external and internal loads are critical. For example, musculoskeletal modeling of the third digit shows that the ratio of (internal) tendon load relative to (external) fingertip force and bone load magnitude to fingertip force was 42% and 55% higher, respectively, in a bonobo than a human (Synek et al., 2019). Thus, we propose that loads incurred during flexed-finger postures in human manipulative activities are not of sufficient magnitude to stimulate plasticity in curvature, but are sufficient to cause cortical modeling of the dorsum (in comparatively straight phalanges).

4.5 | Flexor sheath ridges

The development of the FSRs has been linked to arboreal behaviors (Nakatsukasa et al., 2003) and our study supports the hypothesized biomechanical role of the FSR in reducing the strain on the phalangeal shaft (Nguyen et al., 2014). It can be called into question that FSRs will always be the thickest region of cortical bone within a phalanx because it is a bony projection. However, individuals with small FSRs, or with no FSRs, have a shaft that is relatively thicker compared with the phalangeal shaft thickness of individuals with larger FSRs (see individual specimens in Figure S1).

While an experimental study has explained the biomechanical function of the FSRs (Nguyen et al., 2014), ontogenetic development of the FSRs has yet to be studied. Currently there is a lack of evidence explaining the variability of the FSRs and the functional implications of this variability. For example, it is not clear as to why *Gorilla* have the most prominent FSRs among the extant great apes when at least mountain gorillas spend considerably less time engaging in arboreal locomotion than *Pan* and *Pongo* (Doran, 1997). We also observed variation in FSR morphology within *Pan*, with some individuals displaying FSRs that project minimally from the palmar shaft while others are quite prominent. This variation is present within both male and female individuals of *P. paniscus* and *P. troglodytes* and therefore sexual dimorphism and systemic differences in the skeleton within or between these two species cannot explain the differences in FSR morphology. Variation in FSR morphology may related to other aspects of external morphology, particularly the degree of phalangeal curvature. For example, large FSRs of *Gorilla* may be explained by their relatively straight phalanges while smaller FSRs in *Pan* reflect greater phalangeal curvature. More prominent FSRs in *Gorilla* relative to *Pan* might also be related to the larger forces external (body mass) and internal (e.g., tendon loads) that the *Gorilla* phalanges must withstand during knuckle-walking with more prominent FSRs providing a greater surface area to dissipate forces. However, such hypotheses would predict strong correlations in the development of FSR morphology and variation in phalangeal curvature and body mass (e.g., sex differences) that were not clear within our study sample. These hypotheses require experimental and developmental validation on larger sample sizes to confirm the functional implications of this bony morphology.

4.6 | Palmar median bar

Along with the FSRs, the functional morphology and the development of the palmar median bar and its (generally) accompanying lateral fossae are not well understood. The median bar is an anterior extension of cortical bone on the palmar surface and is typically assumed to have a biomechanical function (Tocheri et al., 2008). As such, we expected that the palmar cortical thickness of the phalangeal shaft would have been significantly thicker in taxa that possess well-developed median bars (i.e., *Pongo* and *Gorilla*). However, preliminary analyses on the IP3s of our sample, shows no evidence of a relationship between palmar median bar morphology and phalangeal cortical thickness. An alternate explanation for the presence of palmar median bar is that it is simply a by-product of the hollowing out of the lateral fossae. However, this hypothesis would imply thin cortical bone at the lateral fossae, which was not observed in our sample. Cortical thickness of the lateral fossae is similar to the thickness of the palmar shaft (except for FSRs) across our sample. Nonetheless, the palmar median bar morphology will affect the shape, distribution of load, and therefore the CSG and bending rigidity and strength is likely to be different. Ontogenetic and biomechanical analyses (e.g., via micro-finite element modeling) that allows on to test the potential functional role of these palmar features is needed to improve our understanding of the general form-function relationships and “trade-offs” of phalangeal external and internal morphology.

4.7 | Limitations

There are some limitations to our study that should be acknowledged. First, our study is founded upon the concept of bone functional adaptation (i.e., bone modeling occurs in response to loads incurred during life that influence both external shape and internal structure), but many other factors, such as genetics, age, sex, and hormones, can also influence bone structure (see review in Kivell, 2016). Furthermore, as CSG relies on beam theory (Lieberman et al., 2004), functional interpretations resulting from cross-sectional properties of bones that are less cylindrical (such as the IPs) may not be as robust or straightforward to interpret and thus should be interpreted with caution. However, there is evidence that (e.g., Gosman et al., 2013; Rodriguez et al., 2018) CSG properties of non-cylindrical regions of bone can be successfully linked to function. Ultimately, a thorough investigation into the relationship between external and internal morphology, alongside kinematic and musculoskeletal modeling, is needed to provide a holistic understanding of how great ape manual behaviors are reflected in variation in bone structure.

5 | CONCLUSION

Our results provide a detailed analysis of the internal structure of the great ape intermediate phalanges. Cortical bone structure of the

intermediate phalanges across the extant great apes reflected differences in hand postures during manual behaviors across the taxa and within the hand of each taxon. Results of this study coupled with the known cortical structure of the proximal phalanges, revealed a similar pattern of cortical bone distribution across the proximal and intermediate phalanges but greater load resistance by proximal phalanges. This demonstrates the functional signals that can be gleaned from the cortex of the proximal and intermediate phalanges of digits 2–5, which can be applied to the reconstruction of hand use in fossil hominins. It also highlights the importance of considering variation in external morphological features for the interpretation of the biomechanical environment that leads to variation in internal bone structure.

AUTHOR CONTRIBUTIONS

Samar M. Syeda: Conceptualization (equal); data curation (lead); formal analysis (lead); investigation (lead); methodology (lead); project administration (equal); visualization (lead); writing – original draft (lead); writing – review and editing (lead). **Zewdi J. Tsegai:** Funding acquisition (supporting); investigation (supporting); methodology (supporting); writing – review and editing (equal). **Marine Cazenave:** Investigation (supporting); methodology (supporting); writing – review and editing (equal). **Matthew M. Skinner:** Conceptualization (equal); data curation (supporting); funding acquisition (lead); investigation (supporting); methodology (supporting); resources (lead); software (lead); supervision (supporting); writing – review and editing (equal). **Tracy L. Kivell:** Conceptualization (equal); data curation (supporting); funding acquisition (lead); investigation (supporting); methodology (supporting); project administration (equal); resources (lead); software (lead); supervision (lead); writing – review and editing (lead).

ACKNOWLEDGMENTS

This project has received funding under the European Union's Horizon 2020 research and innovation programme for European Research Council Consolidator Grant #819960 (MMS and TLK) and Marie Skłodowska-Curie Action #101025719 (ZJT). For access to specimens we thank the following individuals/institutions: C. Boesch, Max Planck Institute for Evolutionary Anthropology; J.-J., Hublin, College de France; F. Mayer and C. Funk, Museum für Naturkunde – Leibniz Institute for Evolution and Biodiversity Science; I. Livne, Powell-Cotton Museum; E. Gilissen, Royal Museum for Central Africa; J. Moggi-Cecchi and S. Bortoluzzi, University of Florence; B. Grosskopf, Johann-Friedrich-Blumenback-Institute for Zoology and Anthropology, Georg-August University, Goettingen; V. Volpato, Frankfurt Senckenberg Museum; J. Svoboda, Science Academy of the Czech Republic; I. Herskovitz, Tel Aviv University; M. M. Lahr, the Duckworth Collection, University of Cambridge; A. D. Pascale, Museo Archeologico del Finale; A. Hildred, The Mary Rose Trust. Finally, we thank the editors and three anonymous reviewers whose helpful feedback improved previous versions of this manuscript.

CONFLICT OF INTEREST STATEMENT

The authors declare no conflict of interest.

DATA AVAILABILITY STATEMENT

Copies of all scans are curated by the relevant curatorial institutions that are responsible for the original specimens and access can be requested through each institution. The authors confirm that the data supporting the findings of this study are available from the corresponding author upon reasonable request.

ORCID

Samar M. Syeda  <https://orcid.org/0000-0003-1514-8086>

Zewdi J. Tsegai  <https://orcid.org/0000-0001-9041-4829>

Marine Cazenave  <https://orcid.org/0000-0001-7194-5958>

Tracy L. Kivell  <https://orcid.org/0000-0001-5087-0897>

REFERENCES

- Alba, D. M., Moyà-Solà, S., & Köhler, M. (2003). Morphological affinities of the *Australopithecus afarensis* hand on the basis of manual proportions and relative thumb length. *Journal of Human Evolution*, 44(2), 225–254. [https://doi.org/10.1016/S0047-2484\(02\)00207-5](https://doi.org/10.1016/S0047-2484(02)00207-5)
- Almécija, S., Alba, D. M., & Moyà-Solà, S. (2009). Pierolapithecus and the functional morphology of Miocene ape hand phalanges: Paleobiological and evolutionary implications. *Journal of Human Evolution*, 57(3), 284–297. <https://doi.org/10.1016/j.jhevol.2009.02.008>
- Almécija, S., Alba, D. M., & Moyà-Solà, S. (2012). The thumb of Miocene apes: New insights from Castell de Barberà (Catalonia, Spain). *American Journal of Physical Anthropology*, 148(3), 436–450. <https://doi.org/10.1002/ajpa.22071>
- Almécija, S., Moyà-Solà, S., & Alba, D. M. (2010). Early origin for human-like precision grasping: A comparative study of pollical distal phalanges in fossil hominins. *PLoS One*, 5(7), e11727. <https://doi.org/10.1371/journal.pone.0011727>
- Ayhan, Ç., & Ayhan, E. (2020). Kinesiology of the wrist and the hand. In S. Angin & I. Simsek (Eds.), *Comparative kinesiology of the human body* (pp. 211–282). Academic Press.
- Barak, M. M., Lieberman, D. E., & Hublin, J. J. (2011). A Wolff in sheep's clothing: Trabecular bone adaptation in response to changes in joint loading orientation. *Bone*, 49(6), 1141–1151. <https://doi.org/10.1016/j.bone.2011.08.020>
- Bardo, A., Moncel, M. H., Dunmore, C. J., Kivell, T. L., Pouydebat, E., & Cornette, R. (2020). The implications of thumb movements for Neanderthal and modern human manipulation. *Scientific Reports*, 10(1), 1–12. <https://doi.org/10.1038/s41598-020-75694-2>
- Begun, D. R., Teaford, M. F., & Walker, A. (1994). Comparative and functional anatomy of Proconsul phalanges from the Kaswanga primate site, Rusinga Island. *Journal of Human Evolution*, 26(2), 89–165. <https://doi.org/10.1006/jhev.1994.1008>
- Bird, E. E., Kivell, T. L., & Skinner, M. M. (2021). Cortical and trabecular bone structure of the hominoid capitate. *Journal of Anatomy*, 239(2), 351–373. <https://doi.org/10.1111/joa.13437>
- Bird, E. E., Kivell, T. L., & Skinner, M. M. (2022). Patterns of internal bone structure and functional adaptation in the hominoid scaphoid, lunate, and triquetrum. *American Journal of Biological Anthropology*, 177(2), 266–285. <https://doi.org/10.1002/ajpa.24449>
- Bush, M. E., Lovejoy, C. O., Johanson, D. C., & Coppens, Y. (1982). Hominid carpal, metacarpal, and phalangeal bones recovered from the Hadar Formation: 1974–1977 collections. *American Journal of Physical Anthropology*, 57(4), 651–677. <https://doi.org/10.1002/ajpa.1330570410>
- Case, D. T., & Heilman, J. (2006). New siding techniques for the manual phalanges: A blind test. *International Journal of Osteoarchaeology*, 16(4), 338–346. <https://doi.org/10.1002/oa.826>
- Cazenave, M., Braga, J., Oettlé, A., Pickering, T. R., Heaton, J. L., Nakatsukasa, M., Thackeray, J. F., de Beer, F., Hoffman, J., Dumoncel, J., & Macchiarelli, R. (2019). Cortical bone distribution in the femoral neck of *Paranthropus robustus*. *Journal of Human Evolution*, 135, 102666. <https://doi.org/10.1016/j.jhevol.2019.102666>
- Cazenave, M., & Kivell, T. L. (2023). Challenges and perspectives on functional interpretations of australopith postcrania and the reconstruction of hominin locomotion. *Journal of Human Evolution*, 175, 103304. <https://doi.org/10.1016/j.jhevol.2022.103304>
- Cepriá-Bernal, J., Pérez-González, A., Mora, M. C., & Sancho-Bru, J. L. (2017). Grip force and force sharing in two different manipulation tasks with bottles. *Ergonomics*, 60(7), 957–966. <https://doi.org/10.1080/00140139.2016.1235233>
- Chirchir, H. (2019). Trabecular bone fraction variation in modern humans, fossil hominins and other primates. *The Anatomical Record*, 302(2), 288–305. <https://doi.org/10.1002/ar.23967>
- Cooney, W. P., 3rd, & Chao, E. Y. (1977). Biomechanical analysis of static forces in the thumb during hand function. *The Journal of Bone and Joint Surgery*, 59(1), 27–36.
- Currey, J. D. (2013). In I. Bones (Ed.), *Bones*. Princeton University Press. <https://doi.org/10.1515/9781400849505>
- Day, M. H. (1978). Functional interpretations of the morphology of postcranial remains of early African hominids. In C. J. Jolly (Ed.), *Early hominids of Africa* (pp. 311–345). St Martin's Press.
- De Monsabert, B. G., Rossi, J., Berton, E., & Vigouroux, L. (2012). Quantification of hand and forearm muscle forces during a maximal power grip task. *Medicine and Science in Sports and Exercise*, 44(10), 1906–1916. <https://doi.org/10.1249/MSS.0b013e31825d9612>
- Doden, E. (1993). The relationship between the function and the inner cortical structure of metacarpal and phalangeal bones. In H. Preuschoft & D. J. Chivers (Eds.), *Hands of primates* (pp. 271–284). Springer. https://doi.org/10.1007/978-3-7091-6914-8_19
- Dollar, A. M. (2014). Classifying human hand use and the activities of daily living. In R. Balasubramanian & V. J. Santos (Eds.), *The human hand as an inspiration for robot hand development* (pp. 201–216). Springer. https://doi.org/10.1007/978-3-319-03017-3_10
- Doran, D. M. (1996). Comparative positional behavior of the African apes. In *Great ape societies* (pp. 213–224). Cambridge University Press. <https://doi.org/10.1017/CBO9780511752414.018>
- Doran, D. M. (1997). Ontogeny of locomotion in mountain gorillas and chimpanzees. *Journal of Human Evolution*, 32(4), 323–344. <https://doi.org/10.1006/jhev.1996.0095>
- Doran, D. M., & Hunt, K. D. (1996). Comparative locomotor behavior of chimpanzees and bonobos: Species and habitat differences. In R. W. Wrangham, W. C. McGrew, F. B. M. de Waal, & P. G. Heltne (Eds.), *Chimpanzee cultures* (pp. 93–108). Harvard University Press.
- Dunmore, C. J., Bardo, A., Skinner, M. M., & Kivell, T. L. (2020). Trabecular variation in the first metacarpal and manipulation in hominids. *American Journal of Physical Anthropology*, 171(2), 219–241. <https://doi.org/10.1002/ajpa.23974>
- Dunmore, C. J., Kivell, T. L., Bardo, A., & Skinner, M. M. (2019). Metacarpal trabecular bone varies with distinct hand-positions used in hominid locomotion. *Journal of Anatomy*, 235(1), 45–66. <https://doi.org/10.1111/joa.12966>
- Dunmore, C. J., Skinner, M. M., Bardo, A., Berger, L. R., Hublin, J. J., Pahr, D. H., Rosas, A., Stephens, N. B., & Kivell, T. L. (2020). The position of *Australopithecus sediba* within fossil hominin hand use diversity. *Nature Ecology & Evolution*, 4(7), 911–918. <https://doi.org/10.1038/s41559-020-1207-5>
- Dunmore, C. J., Wollny, G., & Skinner, M. M. (2018). MIA-clustering: A novel method for segmentation of paleontological material. *PeerJ*, 6, e4374. <https://doi.org/10.7717/peerj.4374>
- Feix, T., Romero, J., Schmiedmayer, H. B., Dollar, A. M., & Kragic, D. (2015). The grasp taxonomy of human grasp types. *IEEE Transactions on Human-Machine Systems*, 46(1), 66–77. <https://doi.org/10.1109/THMS.2015.2470657>
- Galletta, L., Stephens, N. B., Bardo, A., Kivell, T. L., & Marchi, D. (2019). Three-dimensional geometric morphometric analysis of the first

- metacarpal distal articular surface in humans, great apes and fossil hominins. *Journal of Human Evolution*, 132, 119–136. <https://doi.org/10.1016/j.jhevol.2019.04.008>
- Georgiou, L., Dunmore, C. J., Bardo, A., Buck, L. T., Hublin, J. J., Pahr, D. H., Stratford, D., Synek, A., Kivell, T. L., & Skinner, M. M. (2020). Evidence for habitual climbing in a Pleistocene hominin in South Africa. *Proceedings of the National Academy of Sciences of the United States of America*, 117(15), 8416–8423. <https://doi.org/10.1073/pnas.1914481117>
- Gosman, J. H., Hubbell, Z. R., Shaw, C. N., & Ryan, T. M. (2013). Development of cortical bone geometry in the human femoral and tibial diaphysis. *The Anatomical Record*, 296(5), 774–787. <https://doi.org/10.1002/ar.22688>
- Gross, T., Kivell, T. L., Skinner, M. M., Nguyen, N. H., & Pahr, D. H. (2014). A CT-image-based framework for the holistic analysis of cortical and trabecular bone morphology. *Palaeontologia Electronica*, 17(3), 1–13. <https://doi.org/10.26879/438>
- Haile-Selassie, Y., & WoldeGabriel, G. (2009). *Ardipithecus kadabba: Late miocene evidence from the Middle Awash, Ethiopia* (Vol. 2). University of California Press.
- Hervé, M. (2022). *RVAideMemoire: Testing and plotting procedures for bio-statistics*. R package version 0.9-81-2. <https://cran.r-project.org/package=RVAideMemoire>
- Hunt, K. D. (1991). Mechanical implications of chimpanzee positional behavior. *American Journal of Physical Anthropology*, 86(4), 521–536. <https://doi.org/10.1002/ajpa.1330860408>
- Hunt, K. D. (1992). Positional behavior of Pan troglodytes in the Mahale mountains and Gombe stream national parks, Tanzania. *American Journal of Physical Anthropology*, 87(1), 83–105. <https://doi.org/10.1002/ajpa.1330870108>
- Hunt, K. D. (2020). *Chimpanzee: Lessons from our sister species*. Cambridge University Press.
- Inouye, S. E. (1994). Ontogeny of knuckle-walking hand postures in African apes. *Journal of Human Evolution*, 26(5–6), 459–485. <https://doi.org/10.1006/jhevol.1994.1028>
- Jungers, W. L., Godfrey, L. R., Simons, E. L., & Chatrath, P. S. (1997). Phalangeal curvature and positional behavior in extinct sloth lemurs (Primates, Palaeopropithecidae). *Proceedings of the National Academy of Sciences of the United States of America*, 94(22), 11998–12001. <https://doi.org/10.1073/pnas.94.22.11998>
- Karakostis, F. A., Hotz, G., Scherf, H., Wahl, J., & Harvati, K. (2017). Occupational manual activity is reflected on the patterns among hand entheses. *American Journal of Physical Anthropology*, 164(1), 30–40. <https://doi.org/10.1002/ajpa.23253>
- Karakostis, F. A., Hotz, G., Tzouroukis, V., & Harvati, K. (2018). Evidence for precision grasping in Neandertal daily activities. *Science Advances*, 4(9), eaat2369. <https://doi.org/10.1126/sciadv.aat2369>
- Kivell, T. L. (2016). A review of trabecular bone functional adaptation: what have we learned from trabecular analyses in extant hominoids and what can we apply to fossils?. *Journal of Anatomy*, 228(4), 569–594. <https://doi.org/10.1111/joa.12446>
- Kivell, T. L., Baraki, N., Lockwood, V., Williams-Hatala, E. M., & Wood, B. A. (2022). Form, function and evolution of the human hand. *American Journal of Biological Anthropology*, 181(S76), 6–57. <https://doi.org/10.1002/ajpa.24667>
- Kivell, T. L., Barros, A. P., & Smaers, J. B. (2013). Different evolutionary pathways underlie the morphology of wrist bones in hominoids. *BMC Evolutionary Biology*, 13, 1–12. <https://doi.org/10.1186/1471-2148-13-229>
- Kivell, T. L., Churchill, S. E., Kibii, J. M., Schmid, P., & Berger, L. R. (2018). The hand of *Australopithecus sediba*. *PaleoAnthropology*, 1, 282–333. <https://doi.org/10.4207/PA.2018.ART115>
- Kivell, T. L., Deane, A. S., Tocheri, M. W., Orr, C. M., Schmid, P., Hawks, J., Berger, L. R., & Churchill, S. E. (2015). The hand of *Homo naledi*. *Nature Communications*, 6(1), 1–9. <https://doi.org/10.1038/ncomms9431>
- Kivell, T. L., Ostrofsky, K. R., Richmond, B. G., & Drapeau, M. S. (2020). Metacarpals and manual phalanges. In *Hominin postcranial remains from Sterkfontein, South Africa, 1936-1995* (p. 106). <https://doi.org/10.1093/oso/9780197507667.003.0009>
- Larson, S. G., Jungers, W. L., Tocheri, M. W., Orr, C. M., Morwood, M. J., Sutikna, T., Awe, R. D., & Djubiantono, T. (2009). Descriptions of the upper limb skeleton of *Homo floresiensis*. *Journal of Human Evolution*, 57(5), 555–570. <https://doi.org/10.1016/j.jhevol.2008.06.007>
- Leijnse, J. N., Spoor, C. W., Pullens, P., & Vereecke, E. E. (2021). Kinematic and dynamic aspects of chimpanzee knuckle walking: Finger flexors likely do not buffer ground impact forces. *Journal of Experimental Biology*, 224(19), jeb236604. <https://doi.org/10.1242/jeb.236604>
- Lieberman, D. E., Polk, J. D., & Demes, B. (2004). Predicting long bone loading from cross-sectional geometry. *American Journal of Physical Anthropology*, 123(2), 156–171. <https://doi.org/10.1002/ajpa.10316>
- Marchi, D. (2005). The cross-sectional geometry of the hand and foot bones of the Hominoidea and its relationship to locomotor behavior. *Journal of Human Evolution*, 49(6), 743–761. <https://doi.org/10.1016/j.jhevol.2005.08.002>
- Marzke, M. W. (1997). Precision grips, hand morphology, and tools. *American Journal of Physical Anthropology*, 102(1), 91–110. [https://doi.org/10.1002/\(sici\)1096-8644\(199701\)102:1%3C91::aid-ajpa8%3E3.0.co;2-g](https://doi.org/10.1002/(sici)1096-8644(199701)102:1%3C91::aid-ajpa8%3E3.0.co;2-g)
- Marzke, M. W., Shrewsbury, M. M., & Horner, K. E. (2007). Middle phalanx skeletal morphology in the hand: Can it predict flexor tendon size and attachments? *American Journal of Physical Anthropology*, 134(2), 141–151. <https://doi.org/10.1002/ajpa.20646>
- Marzke, M. W., Tocheri, M. W., Steinberg, B., Femiani, J. D., Reece, S. P., Linscheid, R. L., Orr, C. M., & Marzke, R. F. (2010). Comparative 3D quantitative analyses of trapeziometacarpal joint surface curvatures among living catarrhines and fossil hominins. *American Journal of Physical Anthropology*, 141(1), 38–51. <https://doi.org/10.1002/ajpa.21112>
- Matarazzo, S. A. (2008). Knuckle walking signal in the manual digits of *Pan* and *Gorilla*. *American Journal of Physical Anthropology*, 135(1), 27–33. <https://doi.org/10.1002/ajpa.20701>
- Matarazzo, S. A. (2013). *Knuckle-walking signal in the manual phalanges and metacarpals of the great apes (Pan and Gorilla)*. PhD Dissertation. University of Massachusetts Amherst. <https://doi.org/10.7275/gcet-On48>
- Matarazzo, S. A. (2015). Trabecular architecture of the manual elements reflects locomotor patterns in primates. *PLoS One*, 10(3), e0120436. <https://doi.org/10.1371/journal.pone.0120436>
- McClure, N. K., Phillips, A. C., Vogel, E. R., & Tocheri, M. W. (2012). Unexpected pollex and hallux use in wild *Pongo pygmaeus wurmbii*. *American Journal of Physical Anthropology*, 147(S54), S208.
- Nakatsukasa, M., Kunimatsu, Y., Nakano, Y., Takano, T., & Ishida, H. (2003). Comparative and functional anatomy of phalanges in *Nacholapithecus kerioi*, a Middle Miocene hominoid from northern Kenya. *Primates*, 44, 371–412. <https://doi.org/10.1007/s10329-003-0051-y>
- Napier, J. R. (1960). Studies of the hands of living primates. *Proceedings of the Zoological Society of London*, 134(4), 647–657. <https://doi.org/10.1111/j.1469-7998.1960.tb05606.x>
- Napier, J. R. (1962). Fossil hand bones from Olduvai Gorge. *Nature*, 196, 409–411. <https://doi.org/10.1038/196409a0>
- Nguyen, N. H., Pahr, D. H., Gross, T., Skinner, M. M., & Kivell, T. L. (2014). Micro-finite element (μ FE) modeling of the siamang (*Symphalangus syndactylus*) third proximal phalanx: The functional role of curvature and the flexor sheath ridge. *Journal of Human Evolution*, 67, 60–75. <https://doi.org/10.1016/j.jhevol.2013.12.008>
- Ogle, D. H., Doll, J. C., Wheeler, A. P., & Dinno, A. (2022). *FSA: Simple fisheries stock assessment methods*. R package version 0.9.4. <https://cran.r-project.org/package=FSA>
- Oksanen, J., Blanchet, F. G., Friendly, M., Kindt, R., Legendre, P., McGlinn, D., Minchin, P. R., O'Hara, R. B., Simpson, G. L., Solymos, P., Stevens, M. H. H., Szoecs, E., & Wagner, H. (2020). *Vegan: Community ecology package*. R package version 2.5-7. <https://CRAN.R-project.org/package=vegan>

- Patel, B. A., & Maiolino, S. A. (2016). Morphological diversity in the digital rays of primate hands. In T. L. Kivell, P. Lemelin, B. G. Richmond, & D. Schmitt (Eds.), *The evolution of the primate hand: Anatomical, developmental, functional, and paleontological evidence* (pp. 55–100). Springer. https://doi.org/10.1007/978-1-4939-3646-5_4
- Pearson, O. M., & Lieberman, D. E. (2004). The aging of Wolff's "law": Ontogeny and responses to mechanical loading in cortical bone. *American Journal of Physical Anthropology*, 125(S39), 63–99. <https://doi.org/10.1002/ajpa.20155>
- Pickering, T. R., Heaton, J. L., Clarke, R. J., & Stratford, D. (2018). Hominin hand bone fossils from Sterkfontein Caves, South Africa (1998–2003 excavations). *Journal of Human Evolution*, 118, 89–102. <https://doi.org/10.1016/j.jhevol.2018.02.014>
- Pontzer, H., Lieberman, D. E., Momin, E., Devlin, M. J., Polk, J. D., Hallgrímsson, B., & Cooper, D. M. L. (2006). Trabecular bone in the bird knee responds with high sensitivity to changes in load orientation. *Journal of Experimental Biology*, 209(1), 57–65. <https://doi.org/10.1242/jeb.01971>
- Preuschoft, H. (1973). Functional anatomy of the upper extremity. In *The chimpanzee* (Vol. 6, pp. 34–120). Krager.
- Profico, A., Bondioli, L., Raia, P., O'Higgins, P., & Marchi, D. (2021). Morphomap: An R package for long bone landmarking, cortical thickness, and cross-sectional geometry mapping. *American Journal of Physical Anthropology*, 174(1), 129–139. <https://doi.org/10.1002/ajpa.24140>
- R Core Team (2021). R: A language and environment for statistical computing. R Foundation for Statistical Computing, Vienna, Austria. <https://www.R-project.org/>
- Remis, M. J. (1998). The gorilla paradox. In E. Strasser, J. G. Fleagle, A. L. Rosenberger, & H. M. McHenry (Eds.), *Primate locomotion* (pp. 95–106). Springer. https://doi.org/10.1007/978-1-4899-0092-0_6
- Richmond, B. G. (1998). Ontogeny and biomechanics of phalangeal form in primates. *PhD dissertation*, State University of New York at Stony Brook.
- Richmond, B. G. (2007). Biomechanics of phalangeal curvature. *Journal of Human Evolution*, 53(6), 678–690. <https://doi.org/10.1016/j.jhevol.2007.05.011>
- Ricklan, D. E. (1987). Functional anatomy of the hand of *Australopithecus africanus*. *Journal of Human Evolution*, 16(7–8), 643–664. [https://doi.org/10.1016/0047-2484\(87\)90018-2](https://doi.org/10.1016/0047-2484(87)90018-2)
- Rodríguez, L., Carretero, J. M., García-González, R., & Arsuaga, J. L. (2018). Cross-sectional properties of the lower limb long bones in the Middle Pleistocene Sima de los Huesos sample (Sierra de Atapuerca, Spain). *Journal of Human Evolution*, 117, 1–12. <https://doi.org/10.1016/j.jhevol.2017.11.007>
- Rose, M. D. (1988). Functional anatomy of the cheiridia. In J. H. Schwartz (Ed.), *Orangutan biology* (pp. 299–310). Oxford University Press.
- Ruff, C., Holt, B., & Trinkaus, E. (2006). Who's afraid of the big bad Wolff?: "Wolff's law" and bone functional adaptation. *American Journal of Physical Anthropology*, 129(4), 484–498. <https://doi.org/10.1002/ajpa.20371>
- Ruff, C. B., Burgess, M. L., Ketcham, R. A., & Kappelman, J. (2016). Limb bone structural proportions and locomotor behavior in AL 288-1 ("Lucy"). *PLoS One*, 11(11), e0166095. <https://doi.org/10.1371/journal.pone.0166095>
- Samuel, D. S., Nauwelaerts, S., Stevens, J. M., & Kivell, T. L. (2018). Hand pressures during arboreal locomotion in captive bonobos (*Pan paniscus*). *Journal of Experimental Biology*, 221(8), jeb170910. <https://doi.org/10.1242/jeb.170910>
- Sancho-Bru, J. L., Mora, M. C., León, B. E., Pérez-González, A., Iserte, J. L., & Morales, A. (2014). Grasp modelling with a biomechanical model of the hand. *Computer Methods in Biomechanics and Biomedical Engineering*, 17(4), 297–310. <https://doi.org/10.1080/10255842.2012.682156>
- Sarmiento, E. E. (1988). Anatomy of the hominoid wrist joint: Its evolutionary and functional implications. *International Journal of Primatology*, 9, 281–345. <https://doi.org/10.1007/BF02737381>
- Sarringhaus, L. A., MacLachy, L. M., & Mitani, J. C. (2014). Locomotor and postural development of wild chimpanzees. *Journal of Human Evolution*, 66, 29–38. <https://doi.org/10.1016/j.jhevol.2013.09.006>
- Schaller, G. E. (1963). *The mountain gorilla: Ecology and behavior*. University of Chicago Press.
- Schmitt, D., Zeininger, A., & Granatosky, M. C. (2016). Patterns, variability, and flexibility of hand posture during locomotion in primates. In T. L. Kivell, P. Lemelin, B. G. Richmond, & D. Schmitt (Eds.), *The evolution of the primate hand: Anatomical, developmental, functional, and paleontological evidence* (pp. 345–369). Springer. https://doi.org/10.1007/978-1-4939-3646-5_13
- Shrewsbury, M. M., Marzke, M. W., Linscheid, R. L., & Reece, S. P. (2003). Comparative morphology of the pollical distal phalanx. *American Journal of Physical Anthropology*, 121(1), 30–47. <https://doi.org/10.1002/ajpa.10192>
- Skinner, M. M., Stephens, N. B., Tsegai, Z. J., Foote, A. C., Nguyen, N. H., Gross, T., Pahr, D. H., Hublin, J. J., & Kivell, T. L. (2015). Human-like hand use in *Australopithecus africanus*. *Science*, 347(6220), 395–399. <https://doi.org/10.1126/science.1261735>
- Stephens, N. B., Kivell, T. L., Pahr, D. H., Hublin, J. J., & Skinner, M. M. (2018). Trabecular bone patterning across the human hand. *Journal of Human Evolution*, 123, 1–23. <https://doi.org/10.1016/j.jhevol.2018.05.004>
- Stern, J. T., Jungers, W. L., & Susman, R. L. (1995). Quantifying phalangeal curvature: An empirical comparison of alternative methods. *American Journal of Physical Anthropology*, 97(1), 1–10. <https://doi.org/10.1002/ajpa.1330970102>
- Stern, J. T., & Susman, R. L. (1983). The locomotor anatomy of *Australopithecus afarensis*. *American Journal of Physical Anthropology*, 60(3), 279–317. <https://doi.org/10.1002/ajpa.1330600302>
- Su, A., & Carlson, K. J. (2017). Comparative analysis of trabecular bone structure and orientation in South African hominin tali. *Journal of Human Evolution*, 106, 1–18. <https://doi.org/10.1016/j.jhevol.2016.12.006>
- Susman, R. L. (1974). Facultative terrestrial hand postures in an orangutan (*Pongo pygmaeus*) and pongid evolution. *American Journal of Physical Anthropology*, 40(1), 27–37. <https://doi.org/10.1002/ajpa.1330400104>
- Susman, R. L. (1979). Comparative and functional morphology of hominoid fingers. *American Journal of Physical Anthropology*, 50(2), 215–236. <https://doi.org/10.1002/ajpa.1330500211>
- Susman, R. L. (2004). *Oreopithecus bambolii*: An unlikely case of hominid like grip capability in a Miocene ape. *Journal of Human Evolution*, 46(1), 105–117. <https://doi.org/10.1016/j.jhevol.2003.10.002>
- Susman, R. L., & Creel, N. (1979). Functional and morphological affinities of the subadult hand (OH 7) from Olduvai Gorge. *American Journal of Physical Anthropology*, 51(3), 311–331. <https://doi.org/10.1002/ajpa.1330510303>
- Susman, R. L., & Stern, J. T. (1979). Telemetered electromyography of flexor digitorum profundus and flexor digitorum superficialis in pan troglodytes and implications for interpretation of the OH 7 hand. *American Journal of Physical Anthropology*, 50(4), 565–574. <https://doi.org/10.1002/ajpa.1330500408>
- Susman, R. L., Stern, J. T., & Jungers, W. L. (1984). Arboreality and bipedality in the Hadar hominids. *Folia Primatologica*, 43(2–3), 113–156. <https://doi.org/10.1159/000156176>
- Syeda, S. M., Tsegai, Z. J., Cazenave, M., Dunmore, C. J., Skinner, M. M., & Kivell, T. L. (2022). Reconstructing hand use in *Australopithecus sediba* and *Homo naledi*: Mapping variation in cortical thickness across the proximal and intermediate phalanges. *PaleoAnthropology*, 2, 588. <https://doi.org/10.48738/2022.iss2.809>
- Syeda, S. M., Tsegai, Z. J., Cazenave, M., Skinner, M. M., & Kivell, T. L. (2023). Cortical bone distribution of the proximal phalanges in great apes: Implications for reconstructing manual behaviours. *Journal of Anatomy*, 243, 1–22. <https://doi.org/10.1111/joa.13918>

- Syeda, S. M., Tsegai, Z. J., Dunmore, C. J., Cazenave, M., Skinner, M. M., & Kivell, T. L. (2021). Inferring hand use in *Australopithecus sediba*: Analysis of the external and internal morphology of hominin proximal and intermediate phalanges. *PaleoAnthropology*, 1, 258. <https://doi.org/10.48738/2021.iss1.75>
- Synek, A., Lu, S. C., Vereecke, E. E., Nauwelaerts, S., Kivell, T. L., & Pahr, D. H. (2019). Musculoskeletal models of a human and bonobo finger: Parameter identification and comparison to in vitro experiments. *PeerJ*, 7, e7470. <https://doi.org/10.7717/peerj.7470>
- Thompson, N. E. (2020). The biomechanics of knuckle-walking: 3-D kinematics of the chimpanzee and macaque wrist, hand and fingers. *Journal of Experimental Biology*, 223(14), jeb224360. <https://doi.org/10.1242/jeb.224360>
- Thompson, N. E., Ostrofsky, K. R., McFarlin, S. C., Robbins, M. M., Stoinski, T. S., & Alméjida, S. (2018). Unexpected terrestrial hand posture diversity in wild mountain gorillas. *American Journal of Physical Anthropology*, 166(1), 84–94. <https://doi.org/10.1002/ajpa.23404>
- Thorpe, S. K., & Crompton, R. H. (2006). Orangutan positional behavior and the nature of arboreal locomotion in Hominoidea. *American Journal of Physical Anthropology*, 131(3), 384–401. <https://doi.org/10.1002/ajpa.20422>
- Tocheri, M. W., Orr, C. M., Jacofsky, M. C., & Marzke, M. W. (2008). The evolutionary history of the hominin hand since the last common ancestor of *Pan* and *Homo*. *Journal of Anatomy*, 212, 544–562. <https://doi.org/10.1111/j.1469-7580.2008.00865.x>
- Tocheri, M. W., Orr, C. M., Larson, S. G., Sutikna, T., Jatmiko, Saptomo, E. W., Due, R. A., Djubiantono, T., Morwood, M. J., & Jungers, W. L. (2007). The primitive wrist of *Homo floresiensis* and its implications for hominin evolution. *Science*, 317(5845), 1743–1745. <https://doi.org/10.1126/science.1147143>
- Tsegai, Z. J., Kivell, T. L., Gross, T., Nguyen, N. H., Pahr, D. H., Smaers, J. B., & Skinner, M. M. (2013). Trabecular bone structure correlates with hand posture and use in hominoids. *PLoS One*, 8(11), e78781. <https://doi.org/10.1371/journal.pone.0078781>
- Tuttle, R. H. (1967). Knuckle-walking and the evolution of hominoid hands. *American Journal of Physical Anthropology*, 26(2), 171–206. <https://doi.org/10.1002/ajpa.1330260207>
- Tuttle, R. H. (1969). Quantitative and functional studies on the hands of the Anthropoidea. I. The Hominoidea. *Journal of Morphology*, 128(3), 309–363. <https://doi.org/10.1002/jmor.1051280304>
- Tuttle, R. H. (1981). Evolution of hominid bipedalism and prehensile capabilities. *Philosophical Transactions of the Royal Society of London B*, 292(1057), 89–94. <https://doi.org/10.1098/rstb.1981.0016>
- Tuttle, R. H., Basmajian, J. V., Regenos, E., & Shine, G. (1972). Electromyography of knuckle-walking: Results of four experiments on the forearm of *Pan gorilla*. *American Journal of Physical Anthropology*, 37(2), 255–265. <https://doi.org/10.1002/ajpa.1330370210>
- Tuttle, R. H., & Watts, D. P. (1985). The positional behavior and adaptive complexes of *Pan gorilla*. In *Primate morphophysiology, locomotor analysis and human bipedalism* (pp. 261–288). University of Tokyo Press.
- Walker, A., Leakey, R. E., & Leakey, R. (Eds.). (1993). *The nariokotome Homo erectus skeleton*. Harvard University Press.
- Wallace, I. J., Burgess, M. L., & Patel, B. A. (2020). Phalangeal curvature in a chimpanzee raised like a human: Implications for inferring arboreality in fossil hominins. *Proceedings of the National Academy of Sciences of the United States of America*, 117(21), 11223–11225. <https://doi.org/10.1073/pnas.2004371117>
- Ward, C. V., Kimbel, W. H., Harmon, E. H., & Johanson, D. C. (2012). New postcranial fossils of *Australopithecus afarensis* from Hadar, Ethiopia (1990–2007). *Journal of Human Evolution*, 63(1), 1–51. <https://doi.org/10.1016/j.jhevol.2011.11.012>
- Williams-Hatala, E. M., Hatala, K. G., Hiles, S., & Rabey, K. N. (2016). Morphology of muscle attachment sites in the modern human hand does not reflect muscle architecture. *Scientific Reports*, 6(1), 28353. <https://doi.org/10.1038/srep28353>
- Wunderlich, R. E., & Jungers, W. L. (2009). Manual digital pressures during knuckle-walking in chimpanzees (*Pan troglodytes*). *American Journal of Physical Anthropology*, 139(3), 394–403. <https://doi.org/10.1002/ajpa.20994>
- Zeininger, A., Patel, B. A., Zipfel, B., & Carlson, K. J. (2016). Trabecular architecture in the StW 352 fossil hominin calcaneus. *Journal of Human Evolution*, 97, 145–158. <https://doi.org/10.1016/j.jhevol.2016.05.009>
- Zheng, J. Z., De La Rosa, S., & Dollar, A. M. (2011). An investigation of grasp type and frequency in daily household and machine shop tasks. In *IEEE international conference on robotics and automation* (Vol. 2011, pp. 4169–4175). IEEE. <https://doi.org/10.1109/ICRA.2011.5980366>

SUPPORTING INFORMATION

Additional supporting information can be found online in the Supporting Information section at the end of this article.

How to cite this article: Syeda, S. M., Tsegai, Z. J., Cazenave, M., Skinner, M. M., & Kivell, T. L. (2024). Cortical bone architecture of hominid intermediate phalanges reveals functional signals of locomotion and manipulation. *American Journal of Biological Anthropology*, e24902. <https://doi.org/10.1002/ajpa.24902>